Molecular Cell
Article

The Mechanism of a Neurotransmitter:Sodium Symporter—Inward Release of Na^+ and Substrate Is Triggered by Substrate in a Second Binding Site

Lei Shi,[1,2,7] Matthias Quick,[3,6,7] Yongfang Zhao,[3] Harel Weinstein,[1,2] and Jonathan A. Javitch[3,4,5,6,*]
[1]Department of Physiology and Biophysics
[2]HRH Prince Alwaleed Bin Talal Bin Abdulaziz Alsaud Institute for Computational Biomedicine
Weill Medical College of Cornell University, 1300 York Avenue, New York, NY 10021, USA
[3]Center for Molecular Recognition
[4]Department of Psychiatry
[5]Department of Pharmacology
Columbia University College of Physicians and Surgeons, 630 West 168th Street, New York, NY 10032, USA
[6]Division of Molecular Therapeutics, New York State Psychiatric Institute, New York, NY 10032, USA
[7]These authors contributed equally to this work
*Correspondence: jaj2@columbia.edu
DOI 10.1016/j.molcel.2008.05.008

SUMMARY

Eukaryotic neurotransmitter:sodium symporters (NSSs), targets for antidepressants and psychostimulants, terminate neurotransmission by sodium-driven reuptake. The crystal structure of $LeuT_{Aa}$, a prokaryotic NSS homolog, revealed an occluded state in which one leucine and two Na^+ ions are bound, but provided limited clues to the molecular mechanism of transport. Using steered molecular dynamics simulations, we explored the substrate translocation pathway of LeuT. We identified a second substrate binding site located in the extracellular vestibule comprised of residues shown recently to participate in binding tricyclic antidepressants. Binding and flux experiments showed that the two binding sites can be occupied simultaneously. The substrate in the secondary site allosterically triggers intracellular release of Na^+ and substrate from the primary site, thereby functioning as a "symport effector." Because tricyclic antidepressants bind differently to this secondary site, they do not promote substrate release from the primary site and thus act as symport uncouplers and inhibit transport.

INTRODUCTION

Neurotransmitter:sodium symporters (NSSs) play an essential role in the nervous system by terminating synaptic transmission and recycling neurotransmitters for reuse (Rudnick, 2002). These proteins are secondary active transporters that utilize the Na^+ gradient across the plasma membrane to catalyze the uptake of a variety of neurotransmitters from the extracellular milieu against their concentration gradient in a cotransport (symport) mechanism (Torres et al., 2003). NSS substrates include biogenic amines, such as dopamine, norepinephrine, and serotonin, as well as amino acids (γ-aminobutyric acid, glycine, and proline) and osmolytes (betaine and creatine) (Sonders et al., 2005). The transporters for the biogenic amines dopamine, norepinephrine, and serotonin (DAT, NET, and SERT, respectively) are of particular interest because they are targeted by numerous drugs, including the widely abused psychostimulants cocaine and amphetamine (Amara and Sonders, 1998), as well as antidepressants (Iversen, 2006).

Genes encoding more than 200 putative NSS homologs have been computationally identified in prokaryotic genomes (Beuming et al., 2006), and several of these, including TnaT (Androutsellis-Theotokis et al., 2003), LeuT (Yamashita et al., 2005), Tyt1 (Quick et al., 2006), and MhsT (Quick and Javitch, 2007) were shown to be Na^+-dependent amino acid transporters. The crystal structure of LeuT at 1.65 Å resolution revealed an occluded binding pocket with L-leucine (Leu) and two Na^+ ions, Na1 and Na2, complexed within an extensive network of backbone and side-chain interactions, which for Na1 also includes the carboxylate of the bound substrate Leu (Yamashita et al., 2005).

A stoichiometry of 2 Na^+:1 substrate molecules per transport cycle has been inferred for most NSS (Gu et al., 1994), and this has been supported by direct flux experiments in GAT-1 (Krause and Schwarz, 2005). It is likely that coordinated conformational changes couple the movement of Na^+ down its electrochemical gradient to the uphill movement of substrate (Jardetzky, 1966). We have shown (Quick et al., 2006) that Na^+ produces conformational changes consistent with an "outward-facing" conformation and that its absence promotes increased accessibility of cytoplasmic residues consistent with an "inward-facing" conformation of the transporter. Nonetheless, how these changes might drive transport remained a mystery.

The dynamic properties of protein-ligand interaction complexes have been shown to be well described with the current methods of molecular dynamics (MD) simulations (Karplus and Kuriyan, 2005; Kong and Karplus, 2007). However, characterization of the complex conformational rearrangements associated

with physiologically relevant allosteric mechanisms, such as transport by NSS, requires other types of simulation approaches capable of describing dynamics involving barrier crossings. Therefore, we have used steered MD (SMD) simulations (Israelewitz et al., 2001) to study the dynamics of ligand movement in LeuT. SMD had been used to simulate unbinding or unfolding events in several biomolecular systems, e.g., LacY (Jensen et al., 2007). We used this approach to simulate ligand motion in LeuT by pulling the substrate along a simulated pathway. The energy barrier crossings are accelerated by this SMD procedure through the application of external forces. Thus, nanoseconds trajectories of SMD will reasonably simulate molecular behavior during the natural transport process (Jensen et al., 2007), such as transport by NSS, in which turnover occurs over hundreds of milliseconds to seconds.

Combining the computational studies with experimental analysis of dissociation kinetics, transport, and binding, we were able to probe the molecular mechanism of LeuT-mediated substrate translocation. Our findings identified a secondary substrate binding site at the extracellular vestibule of LeuT and revealed the nature of its involvement in the transport mechanism. Very recently, tricyclic antidepressants (TCAs) have been shown to bind to a similar site in LeuT where they were considered to trap the substrate Leu in the occluded binding site (Singh et al., 2007; Zhou et al., 2007). We show here that two substrate molecules can bind simultaneously to the primary and secondary sites and that binding of substrate in the secondary site is the trigger for inward transport of Na^+ and substrate from the primary binding site along the permeation pathway. We propose an allosteric mechanism of Na^+-coupled symport in which binding of substrate to the secondary site is essential for coupling the energy from the electrochemical ion (Na^+) gradient to the transport of solutes by the NSS.

RESULTS

Identification of a Secondary Substrate Binding Site from Steered Molecular Dynamics Simulations

For the SMD simulations, we constructed and equilibrated a molecular system consisting of Leu-bound LeuT immersed in a solvated lipid bilayer, based on the original LeuT crystal structure (Yamashita et al., 2005). At the end of a 24 ns unconstrained equilibration, the LeuT model was very similar to the LeuT crystal structure (rmsd of 1.4 Å), and the transmembrane segments (TMs) 1, 3, 6, and 8 were even closer to that structure (rmsd 0.7 Å). Pulling the substrate from its occluded binding site (termed the primary binding site), known from the LeuT crystal, toward the extracellular milieu with a force applied to the center of mass of the Leu, we identified energy barriers along the simulated path with specific interactions along the pathway. These are mainly ionic interactions and hydrogen bonds between the carboxyl/amine groups of Leu and LeuT residues (for details and representative results from SMD runs, see Figure S1 available online). With the reorganization of the protein environment in the path around the pulled substrate, several of the interactions between the amine group of the substrate and LeuT are severed. This allows the Leu to be repositioned between the aromatic rings of $Tyr108^{3.50}$ and $Phe253^{6.53}$ in a cleft that emerges between TMs 1, 3, and 6 before exiting the primary binding site (for indexing system, see Goldberg et al., 2003; Beuming et al., 2006). The most remarkable details of the observed structural response to the relocation in this initial movement are (1) the consistent interaction of the carboxylate of Leu with Tyr108 and (2) the change in both backbone angles and the rotamer of Phe253, which suggests a gating role for this residue in enabling the Leu side chain to exit the binding site. Results from simulations exploring the role of Na^+ (see below) further support this role.

Further relocation of the substrate with SMD led to a local equilibrium site where the pulling force drops dramatically, thus identifying a new favorable position. Here, Leu is at ~+10 Å along the z axis (relative to the primary Leu binding site defined to be at ~0 Å) and is partially exposed to extracellular bulk water. This site at the extracellular vestibule was termed "the secondary binding site" (Figures 1A–1C) and consists of two components: a hydrophobic pocket composed of $Leu29^{1.50}$, $Tyr107^{3.49}$, $Ile111^{3.53}$, $Trp114^{3.56}$, $Ala319^{EL4}$, $Phe320^{EL4}$, $Phe324^{EL4}$, and $Leu400^{10.44}$—which accommodates the Leu side chain—and an ionic cleft composed of the $Asp404^{10.48}$ and $Arg30^{1.51}$ that establish direct ionic interactions with the amine and carboxyl groups of Leu, respectively. Recent direct structural studies show that TCAs bind to a very similar site in the extracellular vestibule of LeuT, with Leu and two Na^+ remaining bound below the TCA in positions nearly identical to the original crystal structure (Singh et al., 2007; Zhou et al., 2007) in which the secondary site is empty and a water molecule is poised to mediate the interaction between Asp404 and Arg30 (Yamashita et al., 2005).

The Impact of Na^+ on the Structure of the Binding Site

Because substrate binding is Na^+ dependent (see Figure S2A), we used MD simulations to explore the structural role of the two Na^+ bound near the Leu by comparing the holocrystal structure to results from simulations of constructs in which the substrate was removed (−Leu) in the presence (+Na) or absence (−Na) of the two Na^+ ions (Figures 1D–1F). A number of local structural changes are observed to occur in the primary binding site in the absence of both Na^+ and Leu (−Na/−Leu). These produce a "filling in" of the binding cavity (see Figure 1 and the Supplemental Results). An important role in the physiological mechanism of the transporter is attributable to these changes, as filling and shielding of the cavity in the absence of Na^+ is likely to be a feature of an inward-open conformation in which the primary binding site is difficult to access from the extracellular environment. In contrast, we found for the "+Na/−Leu" state that water molecules penetrate the cavity and break the Tyr108 to $Ser355^{8.60}$ hydrogen bond in −Na/−Leu by binding to each of them separately. In this manner, the presence of Na^+ opens access to the primary site for the incoming substrate, consistent with the reported conformational dependence of access to position 3.53 (one helical turn above Tyr108) in the biogenic amine transporters (Chen and Rudnick, 2000; Loland et al., 2004).

Our 30 ns long MD simulations cannot reveal all the intervening conformational changes associated with binding of Na^+ and Leu, but the end points make the trends quite clear: (1) in the absence of Na^+, the binding site is shielded from the extracellular milieu, and no water molecules are found within the cavity (Figures 1D

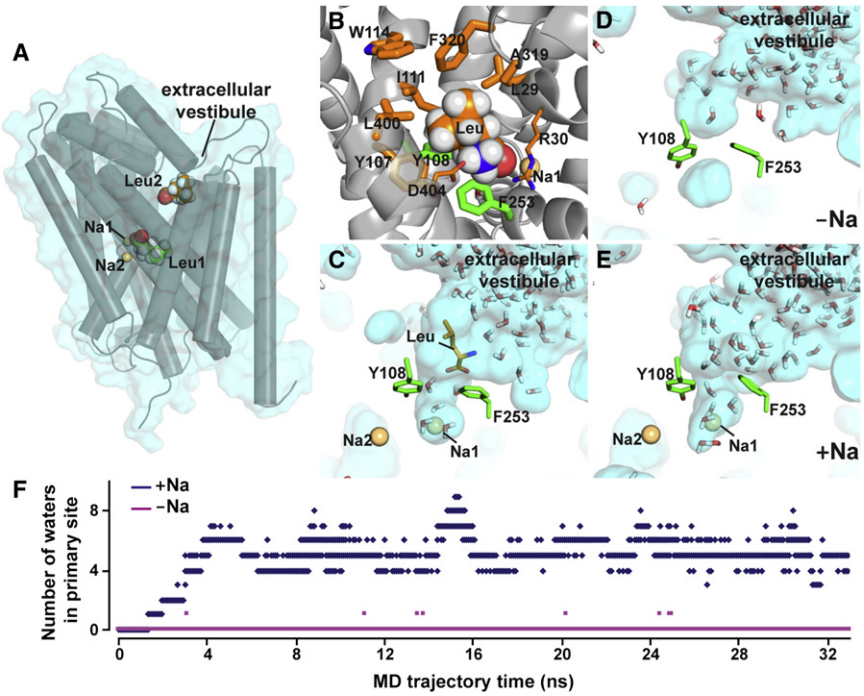

Figure 1. The Secondary Substrate Binding Site in LeuT Identified from SMD Simulations and the Role of Na^+ in the Accessibility of the Primary Site

(A) Side view (perpendicular to the membrane) of a LeuT model (TM helices are shown in cylinder representations) indicating the relative positions of the two binding sites. The secondary binding site is located at the bottom of the extracellular vestibule.

(B) Zoomed-in view of the residues forming the secondary site (in orange); $Tyr108^{3.50}$ and $Phe253^{6.53}$ (in green) line the route connecting the primary site to the secondary site in the SMD simulation (TM11 is omitted to reveal the internal perspective). The charged pair $Arg30^{1.51}$-$Asp404^{10.44}$ is shown in thinner stick rendering.

(C–E) Views of transparent molecular surfaces from the same perspective for various SMD simulation endpoints. (C) shows a representative result from MD equilibration of a final conformation from SMD. (D) and (E) represent the average structures of the −Na/−Leu and +Na/−Leu configurations, respectively.

(F) Time-dependent change in the number of water molecules in the primary binding site calculated from the trajectories of −Na/−Leu and +Na/−Leu, respectively. Note that water fills the primary site in the presence of Na^+, but not in the absence of Na^+. The water entry route in (E) is consistent with the substrate exit route in (C).

and 1F); (2) the presence of Na^+ in the Na1 site organizes/orients TM1 and TM3, -6, and -8 (e.g., the rearranged interactions among $Gly26^{1.47}$, Tyr108, Phe253, and $Ser355^{8.60}$), which facilitates an opening to the extracellular milieu and the entry of water molecules into the site (Figures 1E and 1F); (3) the additional presence of the bound substrate (+Na/+Leu, as in the LeuT crystal structure) protects the primary binding site from direct access from the extracellular milieu through its network of interactions (e.g., with Phe253).

Experimental Evidence for Two Leucines Bound Simultaneously to the Primary and the Secondary Site

To probe the role of the secondary site for Leu observed in the computational studies, we asked whether two substrate molecules can bind simultaneously to the primary and secondary sites and, if so, what the mechanistic implications would be for the function of the transporter. Computational simulations starting from the end of an equilibration trajectory of the crystal structure of LeuT (Yamashita et al., 2005) indicated the feasibility of double occupancy, with a second Leu positioned in the secondary binding site identified in the SMD simulation. The 30 ns simulation converged, with the ligand maintaining its position unchanged for >10 ns in a binding pose in which it interacts directly with Leu400 and Ile111 (Figure S8). Therefore, to create constructs with potentially impaired binding in the secondary binding site, we introduced, one at a time, two mutations: I111C and L400C.

Experimentally, we used a scintillation proximity binding assay (SPA) we described recently (Quick and Javitch, 2007) to quantify the binding of ^{3}H-Leu to purified LeuT in detergent (avoiding the potential complications of removing unbound ^{3}H-Leu). Notably, residual bound Leu would greatly complicate analysis of the stoichiometry of substrate binding. The single Leu bound in the high-resolution structure of LeuT must have come from the bacterial growth media and thus remained bound for several days while LeuT was purified in the absence of Leu (Yamashita et al., 2005). We found, however, that extensive washing of LeuT-containing membranes in the absence of Na^+ removed bound Leu and created an apo-LeuT that has the capacity to bind nearly twice as much ^{3}H-Leu as membranes washed in the presence of Na^+ (Figure S2B). Membranes washed in the absence of Na^+ were used in all subsequent experiments.

At 100 nM ^{3}H-Leu, the secondary site mutants I111C and L400C exhibited ~50% of the ^{3}H-Leu binding observed for WT (Figure 2A). Remarkably, in WT, the stoichiometry at saturating Leu concentration was 1.8 ± 0.1 Leu per LeuT with an EC_{50}^{Leu} of 70 ± 7 nM (Figure 2B, n = 3). In contrast, ^{3}H-Leu bound to I111C and L400C with a stoichiometry of 1.0 ± 0.1 and 0.9 ± 0.1 and an EC_{50}^{Leu} of 105 ± 18 nM and 68 ± 11 nM, respectively (Figure 2B, n = 3). Addition of the TCA clomipramine (CMI) at 1 mM decreased the equilibrium binding of ^{3}H-Leu to WT by 48% ± 3% (n = 4; Figure 2C) but had no effect on equilibrium binding to L400C (Figure 2D) or I111C (data not shown). Taken together, these results are consistent with our hypothesis that Leu can bind simultaneously to the primary binding site and a secondary site. That this secondary site is indeed the site identified in the SMD analysis is supported both by the apparent loss of the second Leu binding in the secondary site mutants and by the ability of the TCA—which binds to the secondary site (Singh et al., 2007; Zhou et al., 2007)—to inhibit binding only to WT but

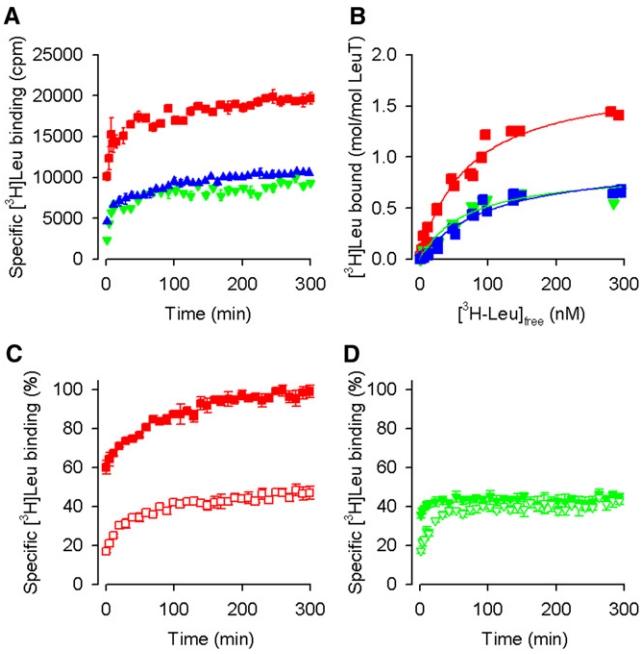

Figure 2. Measurement of Two Leu Binding Sites in LeuT

(A) Time course of 100 nM ^{3}H-Leu binding by WT (solid red square), I111C (solid blue triangle), and L400C (solid green inverted triangle). The half time for binding to equilibrium was 3.7 ± 1 min (n = 5) for WT and 5.3 ± 2.2 min (n = 5) and 9.6 ± 7.5 min (n = 2) for L400C and I111C, respectively.

(B) Stoichiometry of Leu binding. ^{3}H-Leu binding by WT, I111C, and L400C was assayed with 25 ng protein. Three independent experiments were subjected to global fitting in Prism and results of the fits are also shown in the Results.

(C and D) Effect of CMI on Leu association. The time course of 100 nM ^{3}H-Leu binding by WT (C) (open red square, solid red square) and L400C (D) (open green inverted triangle, solid green inverted triangle) was measured in the absence (solid red square, solid green inverted triangle) and presence (open red square, open green inverted triangle) of 1 mM CMI. (A), (C), and (D) show representative experiments that were repeated at least three times, and error bars indicate the mean ± SD of triplicates.

not to constructs that cannot bind ^{3}H-Leu in the mutated secondary site.

Dissociation Experiments Reveal a Kinetic Trapping of Leu

After 30 min incubation, specifically bound ^{3}H-Leu dissociated rapidly from WT or the secondary site mutants regardless of whether the dilution was in the presence (Figure 3A and Figure S3A) or absence of Na^+ (Figure 3B and Figure S3B). Remarkably, we observed that only about 50% of bound ^{3}H-Leu was released when the incubation was carried out for 3–5 hr prior to dilution (data not shown). After prolonged incubation (typically 16 hr—see the Supplemental Experimental Procedures), dissociation from WT into buffer containing Na^+ led to rapid loss of bound ^{3}H-Leu that leveled off at 52% ± 3.7% (n = 4) of total binding (Figure 3C). Thus, it appears that after prolonged incubation, one Leu remains trapped, whereas a second Leu is readily released. This kinetically trapped state likely corresponds to the one visualized in the LeuT crystal structure (Yamashita et al., 2005) and thereby provided us an opportunity to explore the components of the physiological mechanism of transport. Interestingly, ^{3}H-Leu did not dissociate from the mutants in this state when diluted into buffer containing Na^+ (Figure 3C and Figure S3C). This is consistent with the binding and trapping of a single Leu because at the tested concentration ^{3}H-Leu cannot bind to the mutated secondary site. WT differs from the mutants also when release is measured in the absence of Na^+ (mimicking intracellular physiological conditions), because then all bound ^{3}H-Leu dissociates from WT (Figure 3D), whereas in the mutants all the bound ^{3}H-Leu remains trapped (Figure 3D and Figure S3D).

The observed change in ^{3}H-Leu dissociation pattern after prolonged incubation led us to hypothesize that S1 (the substrate in the primary binding site) becomes kinetically trapped in an occluded form of the transporter, as evidenced by the presence of S1 in the crystal structure obtained after purification in the absence of Leu. We further inferred that in order to achieve release of S1, a second substrate (S2) must bind to the secondary site but that release of S1 cannot occur if Na^+ is present (see below experiments supporting the details concerning Na^+ binding and dissociation). In contrast, S2 is readily bound and released from the secondary site, even in the kinetically trapped state. These rules are consistent with (1) the observed dissociation of both S1 and S2 from WT when the transporter is diluted in the absence of Na^+ as well as with (2) the persistent trapping of S1, but not S2, when the transporter is diluted in the presence of Na^+. Based on the behavior of the secondary site mutants, we predicted that emptying the S2 binding site by diluting LeuT-WT in the presence of Na^+ (as in Figure 3C) would prevent the release of S1 upon subsequent dilution into no Na^+; this was indeed found to be the case (Figure 3E). The mutants, which cannot bind S2, mimicked this phenotype, as S1 remained trapped both in the presence and in the absence of Na^+ (Figure 3E and Figure S4A).

In further support of these mechanistic rules, in the absence of Na^+, when 250 nM unlabeled Leu was added to the LeuT-WT trapped state with S1 bound, the secondary site was filled (S2 bound), causing complete release of trapped ^{3}H-Leu (S1) (Figure 3E). In contrast, the identical addition of Leu was without effect in the mutants that disrupt the secondary site (Figure 3E). Interestingly, dissociation from such a mutant, LeuT-L400C, into a very high concentration (1 mM) of Leu recapitulated WT behavior and released ^{3}H-Leu from the S1 binding site (Figure S4A). This suggests that the mechanism of release remains activatable in the mutants if the concentration of Leu is high enough to fill the mutated secondary site.

In the presence of Na^+, when 250 nM unlabeled Leu was added to the WT trapped state with S1 bound, S1 remained trapped (Figure 3G) despite the rebinding of S2 (Figure 3H). This is consistent with the rule (substantiated by the physiological conditions of low intracellular Na^+) that S1 cannot be released in the presence of Na^+ (see below). Supporting this hypothesis, dilution of this species in Na^+-free medium led to release of both S1 (Figure 3G) and of S2 (Figure 3H). Notably, binding of CMI to the secondary site does not have the same effect as substrate. Incubation with 1 mM CMI, which occupies the secondary site (Singh et al., 2007; Zhou et al., 2007) and competes for binding

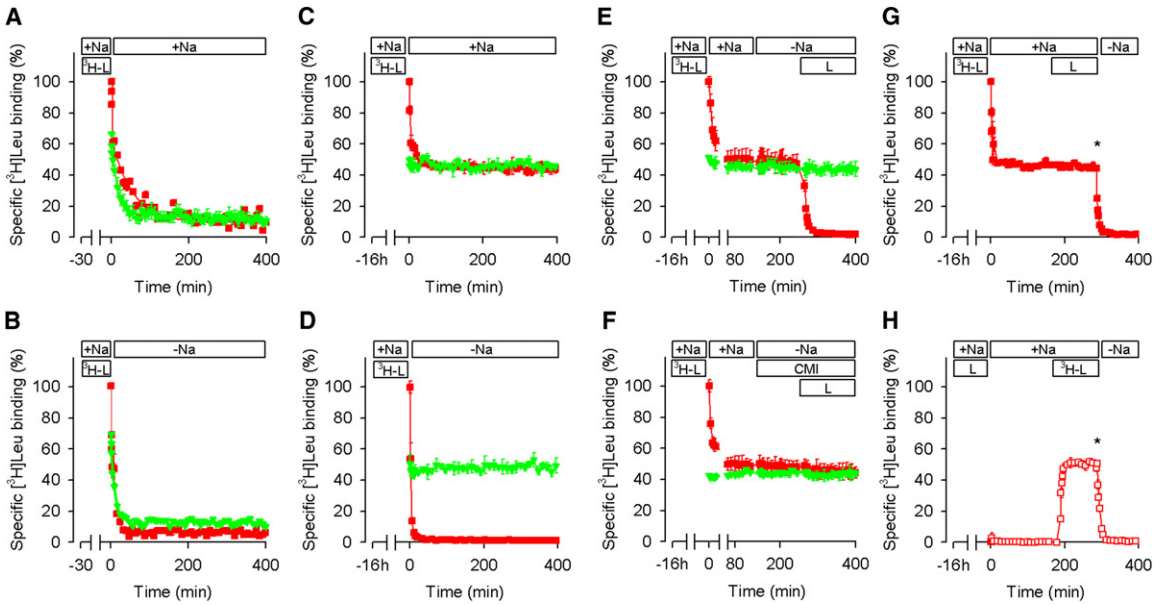

Figure 3. Trapping of Leu in the Primary Binding Site

(A and B) Dissociation of 100 nM ^{3}H-Leu (^{3}H-L) from WT (solid red square) and L400C (solid green inverted triangle) after a 30 min incubation in the presence of 50 mM NaCl (+Na) by dilution in 50 mM NaCl (+Na [A] or NaCl-free media (−Na, [B]). Data points were normalized to the specific binding of WT after a 30 min incubation period.

(C and D) Dissociation of 100 nM ^{3}H-Leu after a 16 hr incubation. The same experimental conditions as in (A) and (B) were applied, and data points were normalized to WT specific binding after 16 hr.

(E) Release of trapped ^{3}H-Leu is triggered by the addition of Leu in the absence of NaCl. After a 16 hr incubation of WT or L400C in the presence of 100 nM ^{3}H-Leu and 50 mM NaCl, the samples were diluted in 50 mM NaCl-medium (+Na) followed by dilution in NaCl-free medium (−Na) and the addition of 250 nM Leu (L).

(F) Effect of CMI on trapped ^{3}H-Leu release. The same experiment as in (E) was performed except that the second dilution was in NaCl-free buffer containing 1 mM CMI. Symbol usage is consistent in (A)–(F).

(G and H) Release of ^{3}H-Leu from the S1 and S2 sites (see text for details) exhibits different dissociation kinetics. After a 16 hr incubation of LeuT-WT with 100 nM ^{3}H-Leu (G) or 500 nM Leu (H) in the presence of 50 mM NaCl, the samples were diluted in 50 mM NaCl medium (+Na) to release bound S2. After reaching steady-state binding levels, the empty S2 site was refilled with 100 nM Leu (G) or 100 nM ^{3}H-Leu (H). Dilution of the equilibrated samples in NaCl-free medium (−Na) caused release of S1 and S2. Thus, the dissociation of S1 is monitored in (G), whereas the dissociation of S2 is monitored in (H). The star in (G) and (H) indicates the 0 min point of the time-normalized data in Figure S7. (A)–(H) show representative experiments that were repeated at least three times, and error bars indicate the mean ± SD of triplicates.

with S2 (but not S1) (Figures 2C and 2D), completely blocked dissociation of S1 in the absence of Na^+ (Figure 3F). Thus, occupation of the secondary site by a TCA is functionally similar to an empty or mutated secondary site, consistent with the behavior of these compounds as transport inhibitors.

Measuring Binding of $^{22}Na^+$ to LeuT Reveals Trapping by Leu

Given the physiological function of the NSS, we expected that different patterns of release and exchange of the two sodiums account for the differential dissociation of ^{3}H-Leu in Na^+/Na^+-free media. Therefore, we used the SPA to measure $^{22}Na^+$ binding directly (Figure S5). Competition with unlabeled Na^+ revealed an $IC_{50}^{Na^+}$ of 10.2 ± 1.2 mM with a Hill coefficient of 1.9 ± 0.1 in WT (Figure 4A) and an $IC_{50}^{Na^+}$ of 10.0 ± 0.1 mM and a Hill coefficient of 2.0 ± 0.1 in L400C (Figure 4B), consistent with an $EC_{50}^{Na^+}$ of 10.3 ± 1.3 mM and a Hill coefficient of 1.9 ± 0.3 for WT and an $EC_{50}^{Na^+}$ of 10.1 ± 3.0 mM with a Hill coefficient of 1.7 ± 0.1 for L400C for Na^+ stimulation of ^{3}H-Leu binding (Figure S2A).

After prolonged incubation in the absence of Leu, $^{22}Na^+$ rapidly and completely dissociated from both WT (Figure 4C) and L400C (Figure 4D) upon dilution, regardless of the presence or absence of unlabeled Na^+. When prolonged incubation with $^{22}Na^+$ was performed in the presence of Leu, $^{22}Na^+$ also dissociated completely upon dilution of WT in the absence of Na^+ (which releases both S1 and S2, Figure 3D) (Figure S6A). However, when the secondary site mutant L400C, in which S1 remained trapped (Figure 3D), was diluted in the absence of Na^+, 47% ± 6% (n = 4) of $^{22}Na^+$ was also trapped, consistent with the release of one Na^+ ion and the trapping of one Na^+ ion together with S1 (Figure S6B).

We hypothesized that after trapping S1 in LeuT-WT, removal of S2 would have an effect similar to that of the secondary site mutants, in that one Na^+ ion would also become trapped. To test this prediction, WT was bound overnight in the presence of Leu and $^{22}Na^+$, which led to the trapping of S1. The transporter was diluted into buffer containing $^{22}Na^+$, which led to release of S2 (Figure 3C). When this complex subsequently was diluted in the absence of Na^+, 47% ± 5% (n = 3) of $^{22}Na^+$ remained bound (Figure 4E), again consistent with the dissociation of one Na^+ and the trapping of one Na^+ along with S1. Similar results were observed in L400C (Figure 4E). However, only in WT, but not in

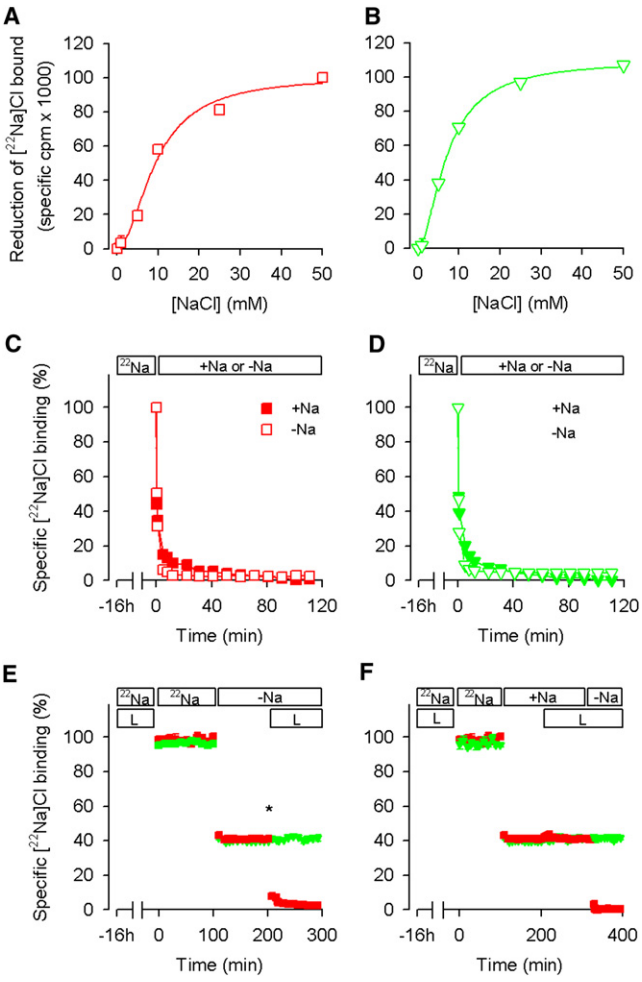

Figure 4. Na^+ Binding Kinetics

(A and B) $^{22}NaCl$ (2 μM) binding by LeuT-WT (A) and L400C (B) was measured with 0–50 mM unlabelled NaCl. Data of two independent experiments were fitted to the Hill equation, and the $IC_{50}^{Na^+}$ and Hill coefficients were shown as mean ± SEM in the Results.

(C and D) Dissociation kinetics of LeuT-WT (C) (open red square, solid red square) and L400C (D) (open green inverted triangle, solid green inverted triangle) after a 16 hr incubation in the presence of 2 μM $^{22}NaCl$ by dilution in 50 mM unlabeled NaCl medium (solid red square, solid green inverted triangle, +Na) or in NaCl-free medium (open red square, open green inverted triangle, −Na).

(E and F) After a 16 hr incubation in the presence of 2 μM $^{22}NaCl$ and 250 nM Leu, LeuT-WT (solid red square) and L400C (solid green inverted triangle) were diluted into 2 μM $^{22}NaCl$-containing medium followed by dilution into NaCl-free medium (−Na) (E) or 50 mM NaCl-containing buffer (+Na) (F) and the addition of 250 nM Leu (in [F], another dilution was done into NaCl-free buffer in the presence of 250 nM L-Leu). The star in (E) indicates the 0 min point of the time normalized data in Figure S7. (C)–(F) show representative experiments that were repeated at least two times, and error bars indicate the mean ± SD of triplicates.

the mutant, was the trapped Na^+ released by subsequent addition of 250 nM Leu and binding of S2; this occurred only in the absence of additional Na^+, but not in the presence of Na^+ (Figures 4E–4F).

These findings reveal a mechanism in which one Na^+ and S1 are trapped in the primary site in the absence of bound S2, but one Na^+ is readily released, presumably to the intracellular side. We have not determined directly which Na^+ (Na1 or Na2) is trapped and which is released, but because only Na1 directly contacts the carboxylate of trapped S1 whereas Na2 is closer to intracellular bulk water, we reasoned that Na1 is the trapped ion and Na2 is released. To evaluate this prediction from a thermodynamic perspective, we compared the free energy for Na1 and Na2 calculated in different conformational states using free energy perturbation (FEP) calculations (see the Experimental Procedures). The calculations also included the solvation energy of Na^+ in a water box (−92.0 ± 0.1 kcal/mol, which agrees with previously reported experimental and computed values; Grossfield et al. [2003]). In the absence of substrate (−S1/−S2/+Na1/+Na2), Na1 and Na2 have free energy of −104.2 and −101.2 kcal/mol, respectively, but with S1 in the primary binding site (+S1/−S2/+Na1/+Na2), the binding of Na2 is weakened (by >4 kcal/mol), whereas Na1 is significantly stabilized (by >8 kcal/mol). Notably, the binding of the substrate(s) lowers the free energy of bound Na2 to resemble that of Na^+ in water, which makes Na2 a much more likely candidate for release. In the absence of Na2 (+S1/−S2/+Na1/−Na2), Na1 is even more stable (by 13 kcal/mol), but the conformational change produced by S2 binding (+S1/+S2/+Na1/−Na2) destabilizes Na1 (by 5 kcal/mol), consistent with the role of S2 in releasing trapped S1 and Na1 in the absence of Na2.

Substrate Binding to the Secondary Site Has a Role in Na^+-Coupled Transport

Alanine (Ala) is transported more efficiently by LeuT than is Leu (Ryan and Mindell, 2007; Singh et al., 2007; Figures 5A and 5B). As a further step in elucidating the physiological relevance of the mechanism we revealed, we extended the study to the effects of Ala on the functions of LeuT. As determined by SPA, the binding stoichiometry of ^3H-Ala to purified LeuT-WT at saturation was 2.0 ± 0.3 (n = 3) Ala per LeuT, whereas for purified L400C it was 1.0 ± 0.2 (n = 3), consistent with our findings with Leu. For WT, the ^3H-Ala binding curve was complex with an EC_{50}^{Ala} of 28.4 ± 5.4 μM (n = 3), whereas the curve for L400C was consistent with a one-site fit with an EC_{50}^{Ala} of 35.8 ± 12.4 μM (n = 3). Unlike Leu, overnight incubation with ^3H-Ala did not lead to substrate trapping (data not shown). However, in the absence of Na^+, 5 μM Ala led to rapid release from WT of trapped ^3H-Leu (Figure 5E) and trapped $^{22}Na^+$ (Figure 5F), consistent with the ability of the Ala substrate to bind to the secondary site and trigger release of S1 and Na1. In contrast, 5 μM Ala was unable to promote release of either S1 (Figure 5E) or Na1 (Figure 5F) from the secondary site mutant L400C.

Functional reconstitution of purified WT and mutant LeuT into proteoliposomes (PLs) was confirmed by ^3H-Ala binding (Figure 5C), which was fully consistent with the binding results in detergent (data not shown). However, despite successful reconstitution, essentially no ^3H-Ala transport into PLs was observed in the secondary site mutants (Figure 5D), in marked contrast to WT. This lack of transport by the secondary site mutants indicates that substrate binding to the secondary site is essential for physiological Na^+-coupled transport and not only for the release of Na1 and S1 in binding assays.

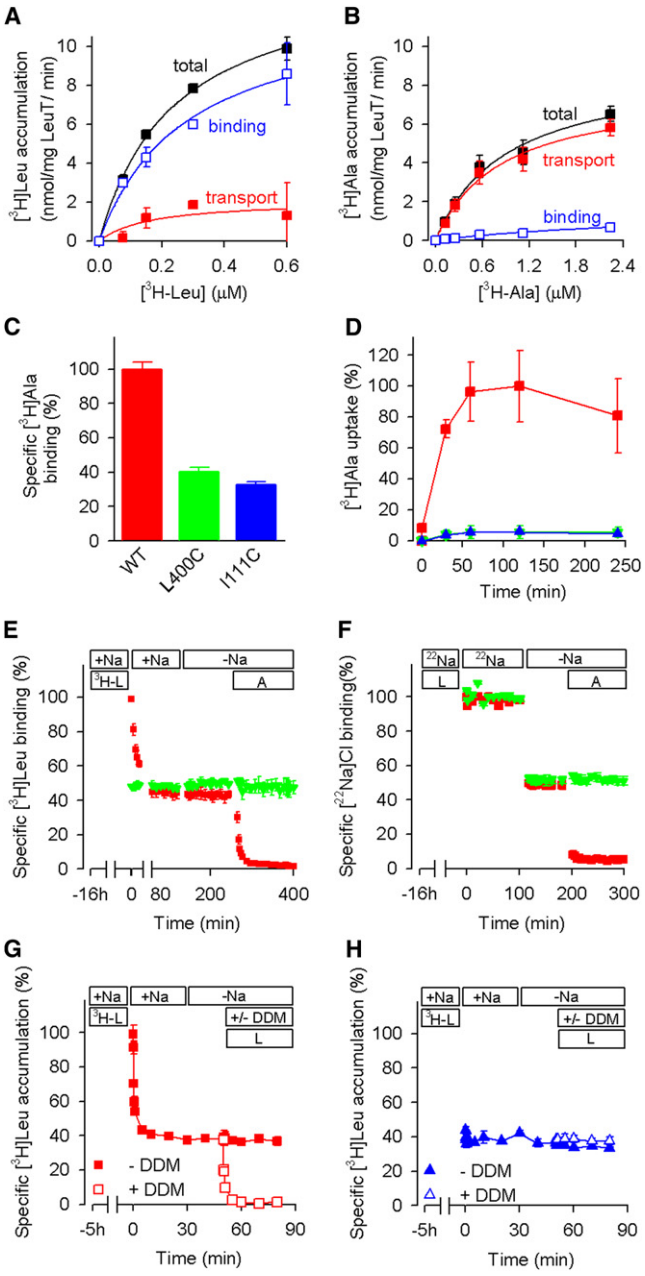

Figure 5. The Secondary Site Is Essential for Transport

(A and B) The activity of LeuT-WT reconstituted into PLs was determined by ^{3}H-Leu (A) and ^{3}H-Ala (B) accumulation with increasing concentrations of either substrate. Measurements were performed in the presence of an inwardly directed Na^+ electrochemical gradient (50 mM external NaCl; solid black square, total accumulation) or by dissipation of the gradient with 25 μg gramicidin/mL (open blue square, specific binding) added 5 min prior to the start of the reaction. Specific substrate transport (solid red square) was determined by the difference of total accumulation and specific binding to exhibit a K_m^{Leu} of 0.16 ± 0.21 μM and V_{max}^{Leu} of 2.1 ± 1 nmol Leu/mg LeuT/min and a K_m^{Ala} of 0.82 ± 0.16 μM and a V_{max}^{Ala} of 8.8 ± 0.7 nmol Ala/mg LeuT/min.

(C) Functional reconstitution of WT (red), L400C (green), and I111C (blue) into proteoliposomes was confirmed by binding of 2 μM ^{3}H-Ala in the presence 50 mM NaCl and gramicidin for 30 min.

(D) Impaired transport by secondary site mutants. Time course of specific ^{3}H-Ala (2 μM final concentration) transport by WT (solid red square), L400C (solid green inverted triangle), and I111C (solid blue triangle) in PLs in the presence of external 50 mM NaCl.

(E and F) Release of trapped ^{3}H-Leu (E) or ^{22}NaCl (F) from WT was triggered by 5 μM Ala. Experimental conditions were identical to those shown in Figure 3E and Figure 4E, respectively, with the exception that Ala was used instead of Leu.

(G and H) Trapped ^{3}H-Leu was released into the lumen of LeuT-WT PLs (G) by the addition of external 250 nM Leu (L) as determined by the loss of radiotracer upon permeabilization of the PLs with 0.05% (w/v) n-dodecyl-β-D-maltopyranoside (DDM). Externally added Leu failed to trigger release of trapped ^{3}H-Leu in PLs with the secondary site mutant L400C (H). Total ^{3}H-Leu accumulation was corrected for nonspecific accumulation in control liposomes. All panels show representative experiments that were repeated two to four times, and errors indicate the mean ± SD of triplicates.

Inward Release of S1 in Response to S2 Binding

To establish that release of trapped S1 was indeed, as depicted in Figure 6, from the cytoplasmic face of the transporter, and thus a measure of the physiological inward release step during the transport cycle, we carried out additional experiments in PLs in which LeuT-WT was reconstituted in an outside-out configuration (see the Supplemental Experimental Procedures). ^{3}H-Leu was bound to the PLs under conditions that allowed trapping of S1. The PLs were diluted in the presence of Na^+, which led to release of S2 but preserved binding of S1 (Figure 5G), just as we observed in detergent (Figure 3C). Subsequent dilution in Na^+-free medium was without further effect on ^{3}H-Leu binding (trapped S1) (Figure 5G), as was also the case in detergent (Figure 3E). In contrast to our results in detergent, however, in the PLs, subsequent addition of 250 nM Leu in the absence of Na^+ did not lead to loss of radioactivity (Figure 5G), since S1 was released to the interior of the PLs and retained upon filtration. That the ^{3}H-Leu (S1) had indeed been released to the inside of the PLs was confirmed by their detergent permeabilization, which led to rapid loss of ^{3}H-Leu upon binding of S2 (Figure 5G). The behavior of the secondary site mutant I111C in the PLs was identical to that in detergent, as S1 remained trapped and was not released (Figure 5H).

To define the intracellular transport pathway through which S1 is released to the cytosplasm, we used an intracellular SMD pulling protocol, as described in the Experimental Procedures. Importantly, in the absence of Na2, it is easier to pull the substrate toward the cytoplasm, as becomes evident from a comparison of force profiles (data not shown). This is consistent with the structural information showing that Na2 is located at the junction of TM1, TM6, and TM8 and likely contributes to the stabilization of the relative orientation of these helices (Figure 6).

In the inward-pulling trajectory, the substrate is surrounded by elements of the N terminus (NT), TM4-IL4-TM5, and TM8 (specifically by Trp8^{NT}, Leu183$^{4.62}$, Ile187^{IL2}, Ile191$^{5.39}$, Ile357$^{8.62}$, and Ala358$^{8.63}$). Notably, in SERT the residues corresponding to Ile187^{IL2} and Ile191$^{5.39}$ have been found to be accessible (Zhang and Rudnick, 2005), and the accessibility of the aligned residue at position 8.63 in GAT1, Cys399$^{8.63}$, is conformationally sensitive (Golovanevsky and Kanner, 1999). The polar portion of Leu interacts directly or through water intermediates with Ala17$^{1.38}$, Gly20$^{1.41}$, and Thr354$^{8.59}$ that is conserved as Thr/Ser in prokaryotic NSS and as Asp in eukaryotic NSS. The identity of the residues swept by the pulled substrate in the SMD procedure are consistent with previous mutagenesis and/or accessibility

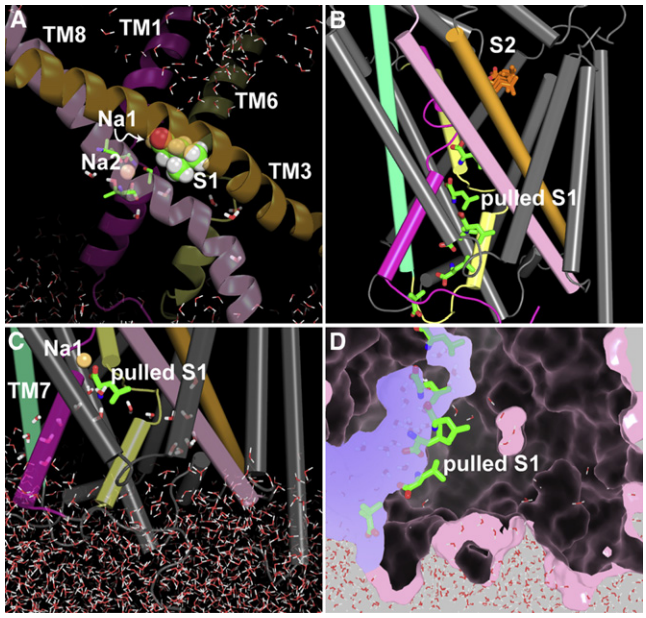

Figure 6. Na2 and the Intracellular Transport Pathway

(A) Positioned at the intersection of the transmembrane segments forming the primary substrate binding site (S1 shown in CPK representation), Na2 has a key role in organizing this region of the transporter. The S1 binding segments TM1, 3, 6, and 8 are shown as ribbons, with Na2 binding residues shown in stick rendering.

(B) The representative poses of S1 (shown in green stick rendering) at different equilibration points from two parallel runs of SMD pulling in the inward (intracellular) direction. These positions are distributed along the SMD pathway, which represents the presumed intracellular substrate translocation pathway (see Table S1 for the residues swept in the pathway). The transmembrane segments are shown as cylinders, and TMs 1, 3, 6, and 8 are colored as in (A).

(C) Viewed from the same angle as in (B), significant water penetration from the intracellular milieu observed in the pathway at the end of the first stage SMD pulling of S1 (see the Supplemental Experimental Procedures). Water molecules penetrate from several directions, including the region between intracellular segments of TMs 1 and 7.

(D) Shown from the same perspective as in (C), the equilibrated structure of a second-stage SMD run is represented as surface rendering obtained as described for Figure 7. An intracellular water tunnel is formed, which is highlighted in light blue, and the progression of the ligand is represented by its position at several points in the SMD trajectory.

studies in other transporters (Table S1), supporting the generality of our findings to other NSS.

The most prominent features of the pathway are described in Figure 6. They are consequences of two main rearrangement groups: one involves the interactions between $Arg5^{NT}$ and $Ser267^{IL3}$/$Tyr268^{IL3}$/$Asp369^{8.74}$ (Kniazeff et al., 2008), and the other is a consequence of the dissociation of the interaction of $Arg11^{1.32}$-$Asp274^{IL3}$. These relate to the movements of entire segments: TM2-IL1 versus IL5-TM11 initiated from the pincer-like Pro-kink of TM2 (Sen et al., 2005); TM6-IL3-TM7 and TM1 versus TM4-IL2-TM5. We observed that the major movements in the protein do not remain localized to the cytoplasmic end of the molecule but are propagated to the region surrounding the secondary site and are much more pronounced in the presence of bound S2 than in its absence. These significant dynamic rearrangements allow penetration of water toward the moving substrate (Figure 6).

DISCUSSION

Our integrated approach of computational MD and SMD simulations combined with corresponding measurements of binding and transport has revealed a functionally essential second substrate binding site in the extracellular vestibule of LeuT. This binding site comprises a hydrophobic portion that interacts with the substrate side chain, and a hydrophilic portion that is partially exposed to bulk water. Residues aligned with the secondary site residues $Leu400^{10.44}$ and $Ile111^{3.53}$ have been suggested to be involved in the substrate translocation pathway in other NSS homologs based on cysteine accessibility data (Keller et al., 2004; Chen and Rudnick, 2000; Loland et al., 2004).

We have now established experimentally that substrate can bind simultaneously to the primary and secondary binding sites. Substrate binding to this secondary site, which we have termed the "symport-effector site," couples the gradient-determined movement of Na^+ to the movement of substrate against its concentration gradient. In this mechanism of Na^+-coupled symport, the second substrate molecule, in the secondary binding site, triggers release of Na^+ and substrate from the primary binding site when Na^+ concentrations are low at the other (cytoplasmic) side. Thus, the combined computational and experimental findings led to a proposed allosteric mechanism for Na^+-coupled symport by this class of proteins, as outlined in Figure 7. According to this mechanism, the transport cycle starts when extracellular Na^+ enables the binding of Na1 and Na2 and the entry of water into the binding site, which reorganizes the primary binding site and shifts the conformational equilibrium of the transporter to an outward-facing conformation. Thus, Na^+ binding increases the affinity of substrate for the primary binding site, and no binding was observed in the absence of Na^+ for Leu (Figure S2A) or Ala (data not shown). When substrate is in the primary binding site, the extracellular gate—composed of $Phe253^{6.53}$, $Arg30^{1.51}$, and $Asp404^{10.48}$—closes and forms a stable interaction, trapping the substrate in the primary site. When Na1 and S1 are occluded in the primary site, we find that the free energy of binding for Na2 is close to its aqueous solvation energy and that Na2 is readily released to the intracellular side. Since the intracellular Na^+ concentration is low, Na2 should rebind only very rarely from the intracellular milieu. But Na1 and S1, which are in direct contact in the crystal structure, remain in the primary site until a second substrate molecule (S2) binds to the symport-effector site and triggers the release of Na1 and substrate from the primary site by disrupting a stabilizing network of interactions (see Figure S8). Both are released from the intracellular side with the support of water penetration (see Figure 6), since the extracellular gate is closed and S2 is bound above it. The physiological Na^+ gradient enables the reentry of Na^+ from the extracellular milieu, which in turn facilitates the reorganization of the outward-facing state. It is likely that the local "effective high concentration" of substrate due to binding in the vestibule helps reload the primary binding site as it is reorganized by Na^+, thereby facilitating the next transport cycle. This mechanism for a secondary transporter supports directional transport of substrate powered by the energy of the Na^+ gradient.

The key role of S2 in this mechanism is substantiated by our findings that mutations of the symport-effector site that abolish

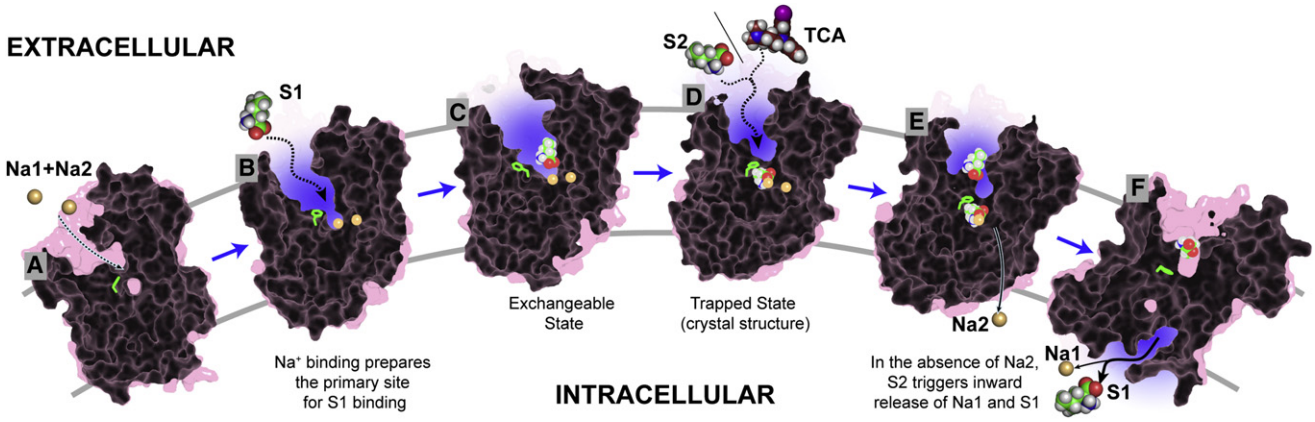

Figure 7. Schematic Model of the Proposed Mechanism of Na^+-Coupled Symport by LeuT

One of the key residues located between the primary and secondary sites, Phe253$^{6.53}$, is shown as a stick model in green because conformational changes in both its backbone and rotamer angles (χ1 rotamer from *gauche*$^-$ [C] to *trans* [D]) are involved in closing the primary site to the extracellular milieu. The transporter models are in molecular surface representations that are sliced open along the proposed transport pathway (shown in greater detail in Figures 1 and 6). A binding/unbinding event that is poised to happen is indicated by a dotted arrow; if it has occurred, the arrow is solid. Enhanced water accessibility is marked by blue surfaces (see Figure 6).

substrate binding there lead to virtually complete loss of transport. Similarly, the transport-inhibiting TCAs, such as CMI, that bind in the secondary site are symport uncouplers, given their ability to compete with, but not mimic, binding of substrate in the symport-effector site. This is likely due to the differences in modes of binding between Leu and CMI in the secondary binding site, which are significant (Figures S8D–S8G). Although our findings are consistent with the ability of TCAs to inhibit roughly half of substrate binding (Zhou et al., 2007; Figure 2C), we cannot define them as noncompetitive antagonists because they compete directly with substrate for binding to the secondary site in LeuT and possibly in NET and SERT as well (Zhou et al., 2007).

The experimental studies underlying the NSS transport mechanism proposed here were made possible by the fact that prolonged binding of Leu and Na^+ leads to a trapped occluded state likely represented by the crystal structure (Yamashita et al., 2005). This stable kinetically trapped state is likely to correspond to what is more typically a transient intermediate conformation in other NSSs. Indeed, Ala, which is reasonably well transported by LeuT in a Na^+-coupled manner, is not trapped within the primary binding site of LeuT but functions as an efficient symport effector at the secondary site (see Figures 5E and 5F). Therefore, the physiological function of other NSSs is likely to follow the mechanistic model described here.

The allosteric mechanism by which binding of a second substrate to the symport-effector site facilitates release of Na1 and S1 is likely complex and involves changes in specific interaction networks (see Figure S8). Experimentally, evidence for coupling between the primary and secondary sites may be apparent in the ^{3}H-Ala binding data and in the fact that the K_m^{Ala} for Ala transport is ~35-fold lower than the EC_{50}^{Ala} for Ala binding. The actual "affinity" of the secondary site for Ala may be higher than observed in an equilibrium binding assay in which binding of Ala to the secondary site may lower its affinity for the primary site. Similar effects in other NSSs may complicate measuring substrate affinity in binding assays with radiolabeled inhibitors. Indeed, this mechanism might account for the lower apparent affinity of biogenic amine substrates determined in competition binding experiments when compared with their apparent K_M for transport (Javitch et al., 1984). Moreover, different affinities of substrates for the primary and symport-effector sites in various transporters may explain a number of other puzzling phenomena, such as inhibitors having different potencies against different substrates (Cesura et al., 1987). Indeed, the ability of serotonin to noncompetitively inhibit dopamine transport by SERT (M.S. Sonders, P. Pörzgen, G.A. Larson, W.O. Woodward, J.A.J., and S.G. Amara, unpublished data) suggests that this happens in human NSS, implying that SERT and other biogenic amine transporters function as described here through an allosteric mechanism involving the two conformationally coupled substrate sites.

EXPERIMENTAL PROCEDURES

Preparation of LeuT, Scintillation Proximity Assay, Transport, and Binding in Proteoliposomes

Expression, purification, and preparation of recombinant LeuT (containing an N-terminal 10-histidine tag) were performed as described in the Supplemental Experimental Procedures. All binding experiments involving purified LeuT variants were performed using the SPA technique, which allows rapid and sensitive measurement of radioisotope binding without the need for a separation step, and transport and binding studies in proteoliposomes were assayed as described (Quick and Javitch, 2007; see also the Supplemental Experimental Procedures for experimental details).

Construction of the Simulated System

The simulations utilized molecular constructs of LeuT based on the crystal structure (Yamashita et al., 2005). Two residues in EL2 and four residues at the beginning of the NT that were not resolved in the crystal structure were added with Modeler (Sali and Blundell, 1993). All the water molecules were maintained in the full-length LeuT model building. The simulation systems with the transporter molecules immersed in explicit water-lipid bilayer-water explicit solvent models were constructed with VMD (Humphrey et al., 1996) and equilibrated with NAMD (Phillips et al., 2005), following a procedure modified from Sotomayor and Schulten (2004). The transporter model was first immersed in a previously equilibrated rectangular patch consisting of 204 POPC

molecules (101 on the periplasmic side and 103 on the cytoplasmic side), one 10 Å layer of water on each side, and Na^+ and Cl^- ions corresponding to a concentration of 150 mM NaCl (a total of ~78,000 atoms). The all-atom CHARMM27 force field was used throughout. Constant temperature (310 K) was maintained with Langevin dynamics, and 1 atm constant pressure was achieved by using the hybrid Nosé-Hoover Langevin piston method on a flexible periodic cell, with orthogonal pressure components—Px, Py, and Pz (perpendicular to membrane)—computed independently to account for system anisotropy. After 24 ns of free equilibration, the LeuT/Leu system reached a final dimension of ~87 × 87 × 98 $Å^3$.

During the equilibration of the protein in its environment, the backbones were initially fixed and then harmonically constrained, and water was prevented from penetrating the protein-lipid interface. Constraints were released gradually in four 300 ps steps with force constants of 1, 0.5, 0.1, and 0.01 kcal/(mol·$Å^2$), respectively. The systems with two substrates bound were obtained by restarting from the last snapshot of the 12 ns "+Na/+Leu" trajectory, with the orientation of Leu in the secondary site taken from the equilibration of SMD (see below) results (overlapping waters were removed before 2500 steps of energy minimization).

All the systems were freely equilibrated for at least 24 ns. At least two independent trajectories were collected for each configuration.

Steered Molecular Dynamics

The constant velocity SMD algorithm implemented in NAMD (Isralewitz et al., 2001) was used in the study designed to identify the residues lining the translocation pathway by dragging the substrates out of the binding site, either upward or downward, at a chosen slow speed. The protein was constrained along the z axis (perpendicular to the membrane plane) during the SMD to avoid its movement in response to the force applied to the substrate in this direction. Constraints were applied to TMs 2, 4, 5, 7, and 9–12—which are not directly involved in substrate binding—in a center of mass scheme. "Center-of-mass pulling" of the substrate was used because preliminary runs showed that steering force applied to the center of mass, as opposed to Cα or Cβ, caused the least distortion of the substrate (data not shown).

The Leu/LeuT system required on average 48 hr to complete a 2 ns SMD run on a system with 32 Intel Xeon CPU (3.20 GHz). For productions runs, the velocity was 0.005 Å/ps, with a force constant of 4 kcal/(mol/$Å^2$) in a pulling direction perpendicular to the membrane plane. During each 2 ns of pulling, constant pressure was maintained with the hybrid Nosé-Hoover Langevin piston method, but the system was decoupled from any thermostat. At the end of each such period the system was coupled to a Langevin thermostat and was equilibrated for at least 8 ns at 310 K.

In the SMD runs, the substrate needs to be pulled slowly enough to allow the transporter to equilibrate in the presence of the substrate in its new position and to reach convergence in terms of the orientation of substrate in the transporter. This requirement is even stronger when the substrate is pulled toward the intracellular side, because the starting (crystal) structure represents an "inward-closed" state. Consequently, we applied two strategies. (1) We divided the inward pulling into three stages: in the first pulling stage, SMD was carried out for 2 ns, followed by 4 ns of MD; in the second, 2 ns of SMD 2 was followed by 20 ns of MD equilibration; finally the substrate is pulled out of the transporter (Jensen et al., 2007). (2) We used gradually reduced pulling velocities in each pulling stage so that the substrate is subjected to a moderate force for longer times (producing small substrate movements).

Free Energy Perturbation

The FEP calculations were carried out with NAMD and the same simulation systems with explicit solvent as described above. For each of the FEP computations, the coupling parameter λ varied from 0 to 1 by increments of 0.05(0.0–1.0) for a total 400 ps for the full annihilation of a Na^+ ion. In the hysteresis tests, the results differed from the annihilation in the same interval by <0.5 kcal/mol. Each reported value is the average of at least two runs starting from different points (after at least 10 ns) of the MD trajectories.

Using the restraining potential approach (Wang et al., 2006), a potential representing the interaction of the Na^+ atom being annihilated with the binding residues at the Na1 or Na2 site was applied, with the form $\frac{1}{2}(k_t[r1 - r1_0] + k_t[r2 - r2_0] + k_a[\theta - \theta_0] + k_a[\Phi - \Phi_0])$. The k_t (100 kcal/mol/$Å^2$) and k_a (100 kcal/mol/rad^2) are force constants for the distance and angle/dihedral restraints, respectively; $r1_0$, $r2_0$, θ_0, and Φ_0 are the reference values averaged from the equilibrated periods of corresponding trajectories (Wang et al., 2006). The resulting restraining energy values were calculated to be in the range of 2.0 to 3.4 kcal/mol, i.e., 2%–3% of the free energies of the Na^+ ions calculated with FEP. The final solvation energies were calculated as the algebraic sum of the FEP and restraining energy values.

The aqueous solvation energy of Na^+ in the simulation system was calculated for direct comparison in a 30 × 30 × 30 $Å^3$ water box containing two Na^+ and two Cl^- ions (equivalent to 123 mM NaCl) using exactly the same FEP/MD procedure as above but without restraints.

SUPPLEMENTAL DATA

The Supplemental Data include Supplemental Experimental Procedures, Supplemental Results, eight figures, one table, and Supplemental References and can be found with this article online at http://www.molecule.org/cgi/content/full/30/6/667/DC1/.

ACKNOWLEDGMENTS

L.S. carried out the computational work, M.Q. performed the binding/transport experiments, and Y.Z. performed transport experiments. We thank Lynn Chung for preparation of membranes and Lihua Duan for making the LeuT-I111C and L400C mutants. We thank Arthur Karlin, Amy Newman, and Ming Zhou for helpful discussion and comments on the manuscript. This work was supported by National Institutes of Health (NIH) grants DA022413, DA017293, and DA012408.

Received: October 23, 2007
Revised: January 17, 2008
Accepted: May 13, 2008
Published: June 19, 2008

REFERENCES

Amara, S.G., and Sonders, M.S. (1998). Neurotransmitter transporters as molecular targets for addictive drugs. Drug Alcohol Depend. *51*, 87–96.

Androutsellis-Theotokis, A., Goldberg, N.R., Ueda, K., Beppu, T., Beckman, M.L., Das, S., Javitch, J.A., and Rudnick, G. (2003). Characterization of a functional bacterial homologue of sodium-dependent neurotransmitter transporters. J. Biol. Chem. *278*, 12703–12709.

Beuming, T., Shi, L., Javitch, J.A., and Weinstein, H. (2006). A comprehensive structure-based alignment of prokaryotic and eukaryotic neurotransmitter/Na^+ symporters (NSS) aids in the use of the LeuT structure to probe NSS structure and function. Mol. Pharmacol. *70*, 1630–1642.

Cesura, A.M., Ritter, A., Picotti, G.B., and Da Prada, M. (1987). Uptake, release, and subcellular localization of 1-methyl-4-phenylpyridinium in blood platelets. J. Neurochem. *49*, 138–145.

Chen, J.G., and Rudnick, G. (2000). Permeation and gating residues in serotonin transporter. Proc. Natl. Acad. Sci. USA *97*, 1044–1049.

Goldberg, N.R., Beuming, T., Soyer, O.S., Goldstein, R.A., Weinstein, H., and Javitch, J.A. (2003). Probing conformational changes in neurotransmitter transporters: a structural context. Eur. J. Pharmacol. *479*, 3–12.

Golovanevsky, V., and Kanner, B.I. (1999). The reactivity of the gamma-aminobutyric acid transporter GAT-1 toward sulfhydryl reagents is conformationally sensitive. Identification of a major target residue. J. Biol. Chem. *274*, 23020–23026.

Grossfield, A., Ren, P., and Ponder, J.W. (2003). Ion solvation thermodynamics from simulation with a polarizable force field. J. Am. Chem. Soc. *125*, 15671–15682.

Gu, H., Wall, S.C., and Rudnick, G. (1994). Stable expression of biogenic amine transporters reveals differences in inhibitor sensitivity, kinetics, and ion dependence. J. Biol. Chem. *269*, 7124–7130.

Humphrey, W., Dalke, A., and Schulten, K. (1996). VMD: visual molecular dynamics. J. Mol. Graph. *14*, 33–38, 27–38.

Israelewitz, B., Gao, M., and Schulten, K. (2001). Steered molecular dynamics and mechanical functions of proteins. Curr. Opin. Struct. Biol. *11*, 224–230.

Iversen, L. (2006). Neurotransmitter transporters and their impact on the development of psychopharmacology. Br. J. Pharmacol. *147* (*Suppl 1*), S82–S88.

Jardetzky, O. (1966). Simple allosteric model for membrane pumps. Nature *211*, 969–970.

Javitch, J.A., Blaustein, R.O., and Snyder, S.H. (1984). [^{3}H]mazindol binding associated with neuronal dopamine and norepinephrine uptake sites. Mol. Pharmacol. *26*, 35–44.

Jensen, M.O., Yin, Y., Tajkhorshid, E., and Schulten, K. (2007). Sugar transport across lactose permease probed by steered molecular dynamics. Biophys. J. *93*, 92–102.

Karplus, M., and Kuriyan, J. (2005). Molecular dynamics and protein function. Proc. Natl. Acad. Sci. USA *102*, 6679–6685.

Keller, P.C., 2nd, Stephan, M., Glomska, H., and Rudnick, G. (2004). Cysteine-scanning mutagenesis of the fifth external loop of serotonin transporter. Biochemistry *43*, 8510–8516.

Kniazeff, J., Shi, L., Loland, C.J., Javitch, J.A., Weinstein, H., and Gether, U. (2008). An intracellular interaction network regulates conformational transitions in the dopamine transporter. J. Biol. Chem. Published online April 21, 2008. 10.1074/jbc.M800475200.

Kong, Y., and Karplus, M. (2007). The signaling pathway of rhodopsin. Structure *15*, 611–623.

Krause, S., and Schwarz, W. (2005). Identification and selective inhibition of the channel mode of the neuronal GABA transporter 1. Mol. Pharmacol. *68*, 1728–1735.

Loland, C.J., Granas, C., Javitch, J.A., and Gether, U. (2004). Identification of intracellular residues in the dopamine transporter critical for regulation of transporter conformation and cocaine binding. J. Biol. Chem. *279*, 3228–3238.

Phillips, J.C., Braun, R., Wang, W., Gumbart, J., Tajkhorshid, E., Villa, E., Chipot, C., Skeel, R.D., Kale, L., and Schulten, K. (2005). Scalable molecular dynamics with NAMD. J. Comput. Chem. *26*, 1781–1802.

Quick, M., and Javitch, J.A. (2007). Monitoring the function of membrane transport proteins in detergent-solubilized form. Proc. Natl. Acad. Sci. USA *104*, 3603–3608.

Quick, M., Yano, H., Goldberg, N.R., Duan, L., Beuming, T., Shi, L., Weinstein, H., and Javitch, J.A. (2006). State-dependent conformations of the translocation pathway in the tyrosine transporter Tyt1, a novel neurotransmitter:sodium symporter from *Fusobacterium nucleatum*. J. Biol. Chem. *281*, 26444–26454.

Rudnick, G. (2002). Mechanisms of Biogenic Amine Neurotransmitter Transporters, Second Edition (Totowa, NJ: Humana Press, Inc.).

Ryan, R.M., and Mindell, J.A. (2007). The uncoupled chloride conductance of a bacterial glutamate transporter homolog. Nat. Struct. Mol. Biol. *14*, 365–371.

Sali, A., and Blundell, T.L. (1993). Comparative protein modelling by satisfaction of spatial restraints. J. Mol. Biol. *234*, 779–815.

Sen, N., Shi, L., Beuming, T., Weinstein, H., and Javitch, J.A. (2005). A pincer-like configuration of TM2 in the human dopamine transporter is responsible for indirect effects on cocaine binding. Neuropharmacology *49*, 780–790.

Singh, S.K., Yamashita, A., and Gouaux, E. (2007). Antidepressant binding site in a bacterial homologue of neurotransmitter transporters. Nature *448*, 952–956.

Sonders, M.S., Quick, M., and Javitch, J.A. (2005). How did the neurotransmitter cross the bilayer? A closer view. Curr. Opin. Neurobiol. *15*, 296–304.

Sotomayor, M., and Schulten, K. (2004). Molecular dynamics study of gating in the mechanosensitive channel of small conductance MscS. Biophys. J. *87*, 3050–3065.

Torres, G.E., Gainetdinov, R.R., and Caron, M.G. (2003). Plasma membrane monoamine transporters: structure, regulation and function. Nat. Rev. Neurosci. *4*, 13–25.

Wang, J., Deng, Y., and Roux, B. (2006). Absolute binding free energy calculations using molecular dynamics simulations with restraining potentials. Biophys. J. *91*, 2798–2814.

Yamashita, A., Singh, S.K., Kawate, T., Jin, Y., and Gouaux, E. (2005). Crystal structure of a bacterial homologue of Na^+/Cl^--dependent neurotransmitter transporters. Nature *437*, 215–223.

Zhang, Y.W., and Rudnick, G. (2005). Cysteine-scanning mutagenesis of serotonin transporter intracellular loop 2 suggests an α-helical conformation. J. Biol. Chem. *280*, 30807–30813.

Zhou, Z., Zhen, J., Karpowich, N.K., Goetz, R.M., Law, C.J., Reith, M.E., and Wang, D.N. (2007). LeuT-desipramine structure reveals how antidepressants block neurotransmitter reuptake. Science *317*, 1390–1393.

Molecular Cell, Volume *30*

Supplemental Data

The Mechanism of a Neurotransmitter:Sodium Symporter—Inward Release of Na^+ and Substrate Is Triggered by Substrate in a Second Binding Site

Lei Shi, Matthias Quick, Yongfang Zhao, Harel Weinstein, and Jonathan A. Javitch

SUPPLEMENTAL EXPERIMENTAL PROCEDURES

Genetic engineering of the leuT gene

In order to facilitate subcloning (introduction of unique restriction sites by silent mutations) we designed a synthetic version of *leuT* which was made by Epoch Biolabs, Inc. The cDNA was introduced into pQ2 (Quick *et al.*, 2006), replacing the entire *tyt1* gene. In the resulting plasmid (named pQO18) *leuT* was under the control of the T5 promoter and encoded a recombinant gene product with an N-terminal 10-histidine tag followed by a TEV cleavage site.

Site-directed replacement of Ile111 and Leu400 by cysteine was performed by standard PCR methods using appropriate mutagenic primers and introduction of the mutagenic fragments into pQO18. The fidelity of all plasmids was confirmed by DNA sequencing (Columbia University).

Purification of LeuT

Expression of recombinant LeuT in *E. coli* C41(DE3) (Miroux and Walker, 1996) (Imaxio), the preparation of membrane vesicles, and the subsequent purification of LeuT

variants was performed as described (Quick and Javitch, 2007) with the exception that PrepEase™ High Yield Histidine purification resin (USB; 1 g resin per 0.5 g of membrane protein) was used for immobilized Ni^{2+}-chelate affinity chromatography. Removal of imidazole or desalting/buffer exchange of the eluted fraction prior to the SPA was performed with Zeba™ desalt spin columns (Pierce). Protein was assayed with different methods as appropriate (Bradford, 1976; Peterson, 1977; Schaffner and Weissmann, 1973).

SPA binding experiments with purified protein in detergent

All binding experiments involving purified LeuT variants were performed using the SPA technique (see Quick and Javitch, 2007). SPA scintillation beads are microspheres containing scintillant that emit light in the blue region of the visible spectrum upon excitation by a radioligand that is held in close enough proximity to the bead. This light is then detected in a photomultiplier tube (PMT) counter. In contrast, if radioactive molecules are free in a solution containing SPA beads, their decay particles will not have sufficient energy to reach the bead and no light will be emitted. This discrimination of binding by proximity means that no separation of bound and free ligand is required.

Purified recombinant LeuT was bound to Cu^{2+} chelate YSi scintillation SPA beads (GE Healthcare) via the N-terminal 10-histidine tag of the protein. 250 µg Cu^{2+} chelate YSi scintillation SPA beads were used per assay in a volume of 100 µL assay buffer composed of either 150 mM Tris/Mes, pH 7.5/20% glycerol/50 mM NaCl/1 mM TCEP/0.1% n-dodecyl-β-D-maltopyranoside ("+Na") or 200 mM Tris/Mes, pH 7.5/20%

glycerol/1 mM TCEP/0.1% n-dodecyl-β-D-maltopyranoside ("-Na") with 250 ng purified LeuT-WT, I111C, or L400C, unless otherwise noted. L-[4,5-^{3}H]Leu (143 Ci/mmol), L-[2,3-^{3}H]alanine [60 Ci/mmol; Moravek), or [^{22}Na]Cl (1017 mCi/mg; Perkin Elmer) was added to the bead solution at the indicated concentration prior to the addition of protein (F=0 format, see manufacturer's instructions). Nonspecific binding was assayed in the presence of 400 mM imidazole. Most experiments were performed with 100 nM ^{3}H-Leu, but preliminary trapping and dissociation results were qualitatively identical when performed at 500 nM ^{3}H-Leu, when the sites would be more fully saturated. All binding assays were performed in 96-well white wall clear-bottom plates and assayed in a Wallac photomultiplier tube MicroBeta™ counter with a 1 min delay between the experimental preparation of the plate and the start of counting. Dissociation/dilution experiments were performed by settling the SPA beads by centrifugation (600 x *g*, 2 min), followed by careful removal of the supernatant and rapid addition of 100 µL assay buffer containing the indicated compounds.

In preliminary experiments (not shown) we discovered that trapping occurs gradually at room temperature and is complete after ~3-5 hours of incubation. Since LeuT, which is from the extreme thermophilic organism *Aquifex aeolicus*, is extremely stable, we used overnight incubations (~16 hours) both to avoid a mixed state (with some transporters already in the trapped state and some not) and to facilitate the long dissociation experiments.

Determination of the binding stoichiometry by SPA

The stoichiometry of radioligand binding to LeuT was determined with the scintillation proximity binding assay. We determined the total moles of purified transporter added based on our experimental determination of protein concentration. 25 ng of purified LeuT variants were used per assay to prevent radioligand depletion; this was far below the binding capacity of the beads. Samples were incubated with increasing concentrations of radioligand and measured in the SPA cpm mode of the MicroBeta^{TM} counter. The efficiency of detection was calculated with a standard curve of known concentration, and this was used to transform cpm into pmol. Specific binding was determined by subtracting the nonspecific binding (as determined in the presence of 400 mM imidazole) from the total binding, and was plotted as a function of free radioligand. Nonlinear regression fitting of the data was performed in Prism 4 to obtain the EC_{50} and molar ratios of ligand-to-LeuT binding. Regardless of any small potential bias introduced by the protein assay or the calculations of counting efficiency, all determinations were subject to the same bias and thus the ratios between the various mutants are reliable.

Transport and Binding in Proteoliposomes

Purified LeuT variants were reconstituted at a 1:150 (w/w) ratio in preformed, Triton X-100 destabilized liposomes that were prepared of *E. coli* polar lipid extract and phosphatidylcholine (both Avanti) at a 3 : 1 (w/w) ratio as described (Quick and Javitch, 2007). The accumulation of ^{3}H-Leu or ^{3}H-Ala was measured at 23 °C in assay buffer composed of 50 mM Tris/Mes, pH 8.5/50 mM NaCl. Binding of ^{3}H-Leu or ^{3}H-Ala to

LeuT proteoliposomes was assayed by dissipating the electrochemical NaCl gradient with 25 μg gramicidin/mL for 5 min prior to the start of the reaction. Uptake/binding reactions were stopped by quenching the samples with ice cold assay buffer followed by rapid filtration through GF/F filters (Advantec MFS, Inc.). Dilution experiments involving LeuT proteoliposomes were performed by diluting 200 μL of a proteoliposome suspension (total of 1 μg protein), which had been preincubated in the presence of gramicidin and 100 nM ^{3}H-Leu in 50 mM Tris/Mes, pH 8.5/20 mM NaCl for the indicated time periods in 60 mL of either 70 mM Tris/Mes, pH 8.5 ("-Na" in Fig. S3 panel E-H) or 50 mM Tris/Mes, pH 8.5/20 mM NaCl ("+Na" in Fig. S3 panel E-H). Five mL of this suspension were filtered through GF/F filters at the appropriate time points.

For release experiments (as shown in Fig. 5 G, H) proteoliposomes were prepared as described above with a protein-to-lipid ratio of 1:200 (w/w). To ensure the use of proteoliposomes with LeuT inserted in an outside-out configuration (with the N-terminal His-tag located internally), the proteoliposomes were preincubated with 1 mg of PrepEase™ High Yield Histidine purification resin per 150 μg reconstituted protein for 30 min at 23 °C. Proteoliposomes containing inversely inserted LeuT (externally located N-terminal His-tag) were removed by settling the resin-bound proteoliposomes (600 x g for 2 min). The orientation of LeuT in the correctly-inserted PL fraction was confirmed by the lack of cleavage of the N-terminal His-tag by TEV protease in intact proteoliposomes, whereas cleavage was complete in 1 % (w/v) n-dodecyl-β-D-maltopyranoside, as assessed by anti-His tag immunoblotting (data not shown). Outside-out LeuT proteoliposomes (and empty liposomes; 50 μg lipids per assay) were incubated in 50 mM Tris/Mes, pH 8.5/50 mM NaCl in the presence of 250 nM ^{3}H-Leu

(after dissipation of the Na^+ gradient by the addition of 25 μg gramicidin per mL 5 minutes prior to the addition of radiotracer) for 5 hours. Unbound ^{3}H-Leu was removed by centrifugation of the (proteo)liposome suspension at 323,000 x g for 20 min. The pellets were resuspended in 50 mM Tris/Mes, pH 8.5/50 mM NaCl/25 μg gramicidin per mL. At the indicated time points 100 μL samples were filtered through GF/F filters followed by washing with 2.5 mL of ice-cold assay buffer. After 1 h, when ^{3}H-Leu binding had reached steady state, the suspension was subjected to an additional ultracentrifugation, the pellets were resuspended in 100 mM Tris/Mes, pH 8.5/25 μg gramicidin per mL, and samples were taken as indicated. After 30 min, during which ^{3}H-Leu binding was stable, 250 nM Leu were added to the (proteo)liposomes in the presence or absence of 0.05 % (w/v) n-dodecyl-β-D-maltopyranoside. This concentration of detergent was chosen based on experiments in which it was found to permeabilize proteoliposomes and release internally accumulated radiotracer, without affecting binding or disrupting the PLs, as determined by a filtration assay (data not shown).

SUPPLEMENTAL RESULTS

MD in the presence and absence of Na^+ (see Figure 1)

In the absence of both Na^+ and Leu in the primary site (-Na/-Leu), the χ1 rotamer of Ser355$^{8.60}$ changes from *gauche*+ to *gauche*-, and the -OH group interacts with the hydroxyl of Tyr108$^{3.50}$, thereby partially occluding the binding cavity and reducing the flexibility of Tyr108 observed in the SMD simulations. Under these conditions, Phe253$^{6.53}$ moves away from TM1 and the Ile359$^{8.63}$ side chain rotates into the binding site, filling it further. Conformational changes in TM1 around the Na^+ binding sites move Gly26$^{1.47}$ closer to Phe253, and reposition Leu25$^{1.46}$, further closing the binding site. Such filling and shielding of the cavity in the absence of Na^+ is likely to be a feature of an inward-facing conformation in which the primary binding site is difficult to access from the extracellular environment. This contrasts with our findings for the "+Na/-Leu" state, in which water molecules penetrate the cavity and break the Tyr108 to Ser355 hydrogen bond by binding to each of them separately. Thus, the presence of Na^+ opens access to the primary site for the incoming substrate.

SUPPLEMENTAL FIGURES

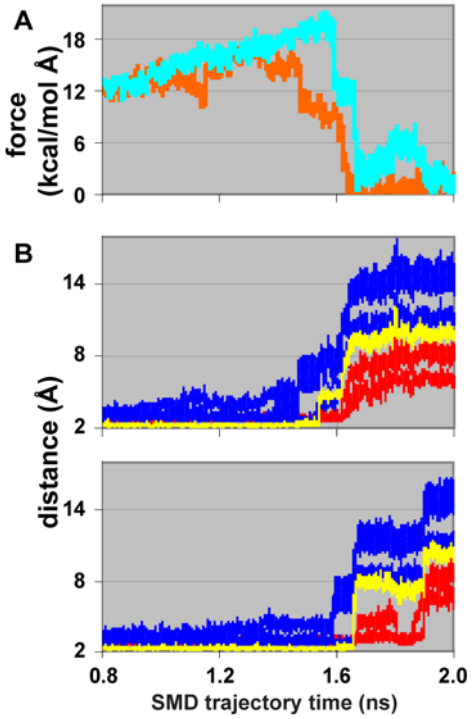

Figure S1. Results from Steered Molecular Dynamics (SMD) simulations of Leu moving in the extracellular direction in a constant-velocity pulling scheme. **A)** The force applied to the center of mass of the Leu as a function of time in two representative runs. **B)** Changes in local interactions of the amine group (N atom) and the carboxyl group (O atom) of the substrate Leu during the same two runs shown in **A**. The evolution in time of average distances (in Å) to the Leu fragments from their corresponding closest interacting neighbors are shown in red for the carboxy group of Leu to Gly26$^{1.47}$ and Tyr108$^{3.50}$; in yellow for the carboxy group of Leu to Na1; and blue for the amine group of Leu to Asn21$^{1.42}$:O, Ala22$^{1.43}$:O, Phe253$^{6.53}$:O, Thr254$^{6.54}$:O, and Ser256$^{6.56}$:Oγ. Note that the sequence of dissociation from these interactions is found to be the same in the two runs: the amine group of Leu dissociates first, followed by the carboxy group of Leu.

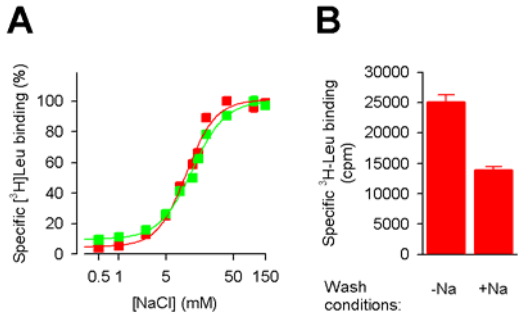

Figure S2. Na^+ dependence of LeuT. **A**) Specific binding of 100 nM ^{3}H-Leu to LeuT-WT (□) and L400C (▼) was assayed in the presence of increasing NaCl concentrations. Fitting the data to the Hill equation revealed an $EC_{50}^{Na^+}$ of 10.3 ± 1.3 with a Hill coefficient of 1.9 ± 0.3 for WT and an $EC_{50}^{Na^+}$ of 10.1 ± 3.0 with a Hill coefficient of 1.7 ± 0.1 for L400C. Kinetic constants are the mean ± S.E.M of the fits of three individual experiments. **B**) Occupation of LeuT with Leu from culture medium. *E. coli* C41(DE3)/pQO18 cells were cultured and membrane vesicles were prepared as described in SUPPLEMENTAL EXPERIMENTAL PROCEDURES. Vesicles were washed at least three times with 200 mM Tris/Mes, pH 7.5 (-Na) or 150 mM Tris/Mes, pH 7.5/50 mM NaCl (+Na) before solubilization with 1 % (w/v) n-dodecyl-β-D-maltopyranoside for 1 h. After centrifugation of the samples (300,000 x g, 30 min, 4°C), the supernatant of each sample (3 µg total protein per assay) was used in an SPA assay (50 nM ^{3}H-Leu in 150 mM Tris/Mes, pH 7.5/50 mM NaCl/20% glycerol/1 mM TCEP/0.1 % (w/v) n-dodecyl-β-D-maltopyranoside).

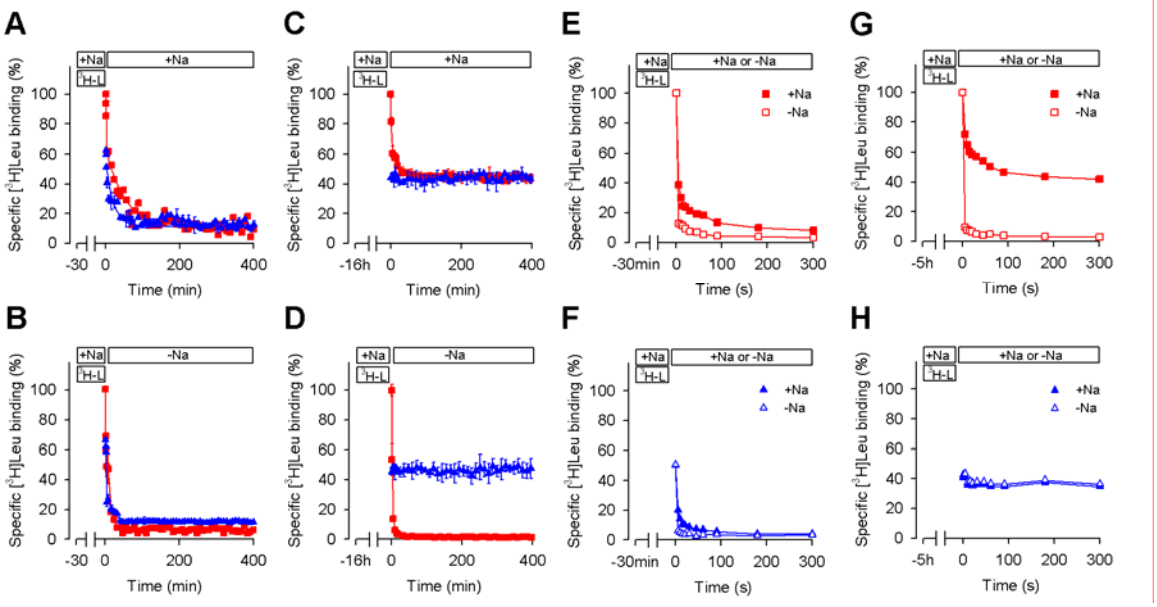

Figure S3. Trapping of S1. **A - D**) Dissociation kinetics of LeuT-WT (□) and I111C (▲) were performed as described in Fig. 3A – D. **E–H**). Dissociation kinetics after preincubation of proteoliposomes containing LeuT-WT (**E**, **G**, □,□) or I111C (**F**, **H**, ▲, △) in the presence of 100 nM ^{3}H-Leu, 20 mM NaCl (+Na), and 25 µg gramicidin/mL for 30 min (**E**, **F**) or 5 h (**G**, **H**). Proteoliposomes were diluted into 50 mM Tris/Mes, pH 8.5/20 mM NaCl (+Na, □,▲) or 70 mM Tris/Mes, pH 8.5 (-Na, □,△). Data are normalized to the ^{3}H-Leu binding level of LeuT-WT after each indicated incubation period.

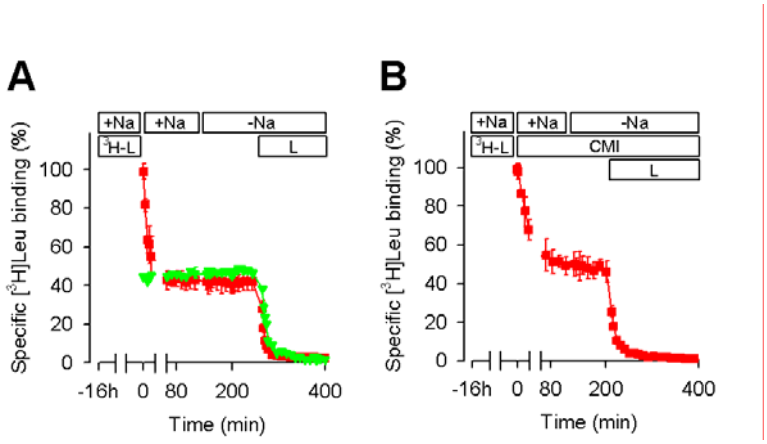

Figure S4. Effect of high Leu concentrations on the release of trapped S1. The experiment shown in **A** was performed identically to that depicted in Fig. 3E with the exception that 1 mM L-Leu rather than 250 nM was added in the final step. In panel **B** the L-Leu concentration was 10 mM as opposed to 250 nM in Fig. 3F. Because TCA binding is reversible, addition of excess Leu to this state led to dissociation of S1 due to competition with the TCA for binding to the secondary site and S2-promoted release of S1.

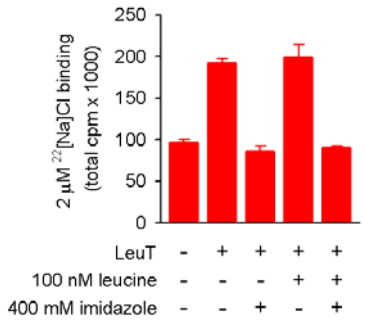

Figure S5. $^{22}Na^{+}$ binding to LeuT. Binding of 2 µM $^{22}NaCl$ by the SPA was assayed under different experimental conditions as indicated. The total amount of bound $^{22}Na^{+}$ was not affected by the presence or absence of 100 nM L-Leu and was reduced to background levels by the addition of 400 mM imidazole in either condition.

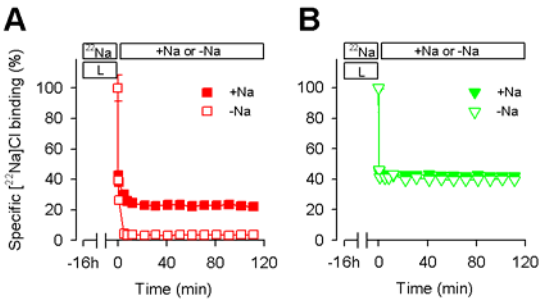

Figure S6. Trapping of Na^+. Dissociation kinetics of LeuT-WT (**A**, □,□) and L400C (**B**,▼,▽) after a 16-h incubation in the presence of 2 µM ^{22}NaCl and 250 nM Leu. Filled symbols (□,▼) indicate dilution in 50 mM unlabeled NaCl-containing assay buffer (+Na) while open symbols (□,▽) indicate dilution in NaCl-free (-Na) buffer. Diluting the Leu-bound WT into Na^+ (which traps S1 in the primary site) resulted in 19±5 % (n=2) trapped $^{22}Na^+$ (**A**), which is interpretable as a kinetic average of competing steps. Na2 dissociates rapidly, and Na1 dissociates as well from those transporter molecules in which S2 is still bound in the absence of Na2, but unlabeled Na1 and Na2 rapidly rebind. However, if Na2 rebinds before Na1 can dissociate, labeled Na1 is trapped. This leads to exchange of all Na2 as well as some fraction of Na1, for a residual of ~20% of the originally bound $^{22}Na^+$. Remarkably, essentially no S1 is lost during this process (Fig. 3C), suggesting that dissociation of S1 is slower than the dissociation of Na1 and the subsequent rebinding of Na1 and Na2 (see Fig. S7).

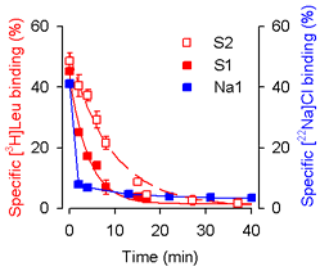

Figure S7. Release of S1, S2, and Na1. Detailed view of the dissociation of S1 (□), S2 (□), and Na1 (□) as shown in Fig. 3G and H, and Fig. 4E, respectively (the 0 min time point is presented with a star in each figure). Data were fitted to a single exponential decay function. The release half-times, $t_{1/2}$, for S1 and S2 were 2.7 ± 0.01 min and 6.8 ± 0.1 min (mean ± SEM of the fit of three individual experiments), respectively, whereas the fast release of $^{22}Na^{+}$ (in all experiments) precluded reliable fitting.

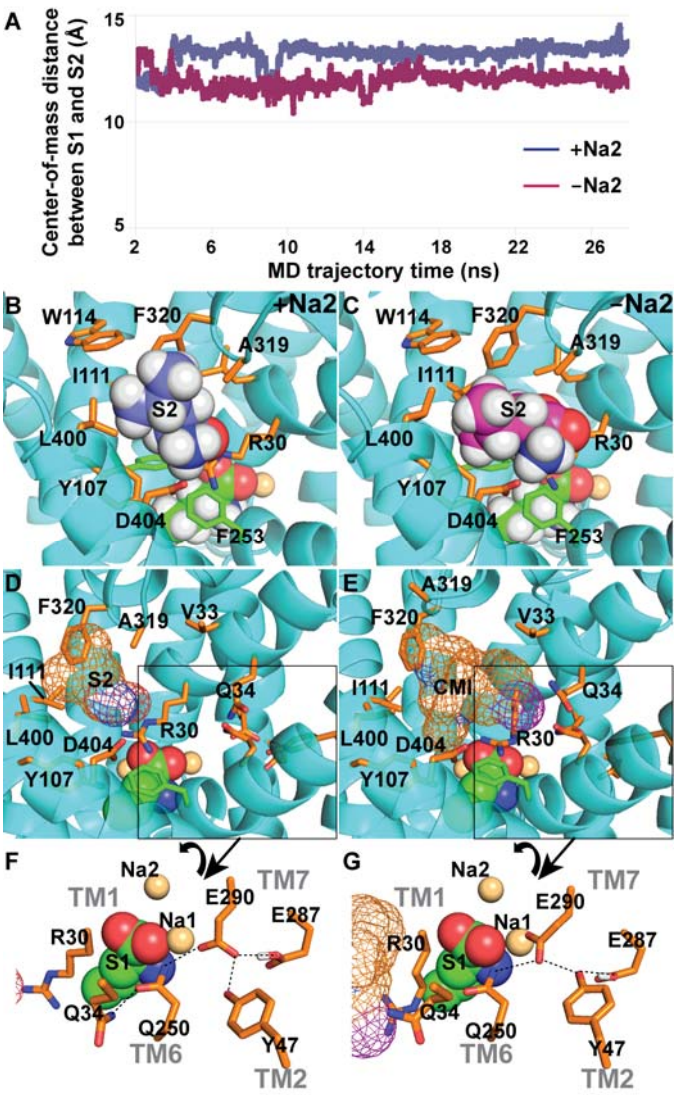

Figure S8. The second Leu (S2) bound in the secondary binding site. **A)** Distance (in Å) between the centers-of-mass of the two substrate molecules, S1 and S2, one in the primary and the other in the secondary site, along the trajectories of two parallel MD equilibrations carried out in the presence (blue) and the absence (purple) of Na2. Note that in the absence of Na2, S2 is consistently closer to S1. **B, C)** The binding poses of S2 (color coding as in Panel A) in the presence (B) and absence (C) of Na2. Note hydrophobic contacts to Ile111 and Leu400. Panels **D** and **E** compare the binding of Leu and a TCA inhibitor, CMI, in the secondary binding site. **D** is a zoomed-out view of

Panel **B**, with S2 in a mesh representation. In **E**, CMI is shown in its position observed crystallographically (Singh *et al.*, 2007) and the comparable positioning relative to **D** is achieved by superimposing the LeuT structures. Compared to S2, CMI makes much more extensive contacts in the bottom of the extracellular vestibule, towards the cleft between TM1 and TM6 and down to the juncture of TM1 and 3. Among these interactions of CMI, the one with Val33$^{1.54}$ and Gln34$^{1.55}$ stabilizes the extracellular portion of TM1. They affect as well a nearby interaction network formed by residues from TM2, 6, and 7. In Panels **F** and **G** (zoomed-in and slightly rotated views as indicated by boxes and arrows) this interaction network is shown to be associated with Na1 binding, and to involve the highly conserved Gln250$^{6.50}$ that forms a hydrogen bond to Arg30 in the crystal structure with only S1 (Yamashita *et al.*, 2005). Notably, the other residue in this network is Glu290$^{7.42}$, whose aligned position has been found to be involved in Cl^- dependence in mammalian NSS (Zomot *et al.*, 2007; Forrest *et al.*, 2007). Hydrogen bonds are indicated by dotted lines. Together, panels D and E, and the extensions shown in panels F and G also reveal the differences observed when Leu or CMI is bound (note the alternative interactions of Glu290 with the highly conserved Tyr47$^{2.40}$ and with nearby Glu287$^{7.39}$).

SUPPLEMENTAL TABLE S1

LeuT residue[index(a)]	Transporter: mutant[b]	Accessibility	Disrupted transport	References
Trp8^{NT}	DAT:W63L	NA[c]	+	Chen *et al.*, 2001; Bennett and Kanner, 1997
Ala17$^{1.38}$	SERT:S91A	+[d]	NA	Henry *et al.*, 2003
Met18$^{1.39}$	Tyt1:C18A	+	NA	Quick *et al.*, 2006
Leu183$^{4.62}$	SERT:I270C	+	NA	Zhang and Rudnick, 2005
Ile187^{IL2}	SERT:V274C	+	NA	Zhang and Rudnick, 2005
Ile191$^{5.39}$	SERT:S277C	+	NA	Zhang and Rudnick, 2005
Ala195$^{5.43}$	SERT:V281C	+	NA	Zhang and Rudnick, 2005
Ala261$^{6.61}$	GAT1:S302C	NA	+	Mari *et al.*, 2006
Ile262$^{6.62}$		NA	NA	
Tyr265$^{6.65}$	Tyt1:C238F	+	NA	Quick *et al.*, 2006
Ala282$^{7.34}$	SERT:T364I	NA	-	Penado *et al.*, 1998
Ile357$^{8.62}$		NA	NA	
Ala358$^{8.63}$	GAT1:C399	+	NA	Golovanevsky and Kanner, 1999
Gln361$^{8.66}$	DAT:E428A	NA	+	Loland *et al.*, 2004

[a] For indexing systems see (Goldberg *et al.*, 2003; Beuming *et al.*, 2006)

[b] The sequence alignment is based on (Beuming *et al.*, 2006).

[c] "NA" indicates that no cysteine accessibility data are available. In the absence of such accessibility data, we indicated whether data were available suggesting that mutation of the aligned residue disrupts transport.

[d] "+" indicates that an endogenous or substituted cysteine at the specified locus reacted with charged methanethiosulfonate derivatives (Karlin and Akabas, 1998). During the intracellular SMD, the identified residues maintain distances within 4Å of the substrate for at least 1.0 ns during the equilibration phases in between the pulling phases. This list

excludes the residues in the primary binding site (see Table 2 of Beuming *et al.*, 2006). The literature information has been collected and organized with TRAC (http://icb.med.cornell.edu/trac).

SUPPLEMENTAL REFERENCES

Bennett, E.R., and Kanner, B.I. (1997). The membrane topology of GAT-1, a (Na^+ + Cl^-)-coupled gamma-aminobutyric acid transporter from rat brain. J Biol Chem *272*, 1203-1210.

Beuming, T., Shi, L., Javitch, J.A., and Weinstein, H. (2006). A comprehensive structure-based alignment of prokaryotic and eukaryotic neurotransmitter/Na^+ symporters (NSS) aids in the use of the LeuT structure to probe NSS structure and function. Mol Pharmacol *70*, 1630-1642.

Bradford, M.M. (1976). A rapid and sensitive method for the quantitation of microgram quantities of protein utilizing the principle of protein-dye binding. Anal Biochem *72*, 248-254.

Chen, N., Vaughan, R.A., and Reith, M.E. (2001). The role of conserved tryptophan and acidic residues in the human dopamine transporter as characterized by site-directed mutagenesis. J Neurochem *77*, 1116-1127.

Forrest, L.R., Tavoulari, S., Zhang, Y.W., Rudnick, G., and Honig, B. (2007). Identification of a chloride ion binding site in Na^+/Cl^--dependent transporters. Proc Natl Acad Sci U S A *104*, 12761-12766.

Goldberg, N.R., Beuming, T., Soyer, O.S., Goldstein, R.A., Weinstein, H., and Javitch, J.A. (2003). Probing conformational changes in neurotransmitter transporters: a structural context. Eur J Pharmacol *479*, 3-12.

Golovanevsky, V., and Kanner, B.I. (1999). The reactivity of the gamma-aminobutyric acid transporter GAT-1 toward sulfhydryl reagents is conformationally sensitive. Identification of a major target residue. J Biol Chem *274*, 23020-23026.

Henry, L.K., Adkins, E.M., Han, Q., and Blakely, R.D. (2003). Serotonin and cocaine-sensitive inactivation of human serotonin transporters by methanethiosulfonates targeted to transmembrane domain I. J Biol Chem *278*, 37052-37063.

Karlin, A., and Akabas, M.H. (1998). Substituted-cysteine accessibility method. Methods Enzymol *293*, 123-145.

Loland, C.J., Granas, C., Javitch, J.A., and Gether, U. (2004). Identification of intracellular residues in the dopamine transporter critical for regulation of transporter conformation and cocaine binding. J Biol Chem *279*, 3228-3238.

Mari, S.A., Soragna, A., Castagna, M., Santacroce, M., Perego, C., Bossi, E., Peres, A., and Sacchi, V.F. (2006). Role of the conserved glutamine 291 in the rat gamma-aminobutyric acid transporter rGAT-1. Cell Mol Life Sci *63*, 100-111.

Miroux, B., and Walker, J.E. (1996). Over-production of proteins in *Escherichia coli*: mutant hosts that allow synthesis of some membrane proteins and globular proteins at high levels. J Mol Biol *260*, 289-298.

Penado, K.M., Rudnick, G., and Stephan, M.M. (1998). Critical amino acid residues in transmembrane span 7 of the serotonin transporter identified by random mutagenesis. J Biol Chem *273*, 28098-28106.

Peterson, G.L. (1977). A simplification of the protein assay method of Lowry *et al*. which is more generally applicable. Anal Biochem *83*, 346-356.

Quick, M., and Javitch, J.A. (2007). Monitoring the function of membrane transport proteins in detergent-solubilized form. Proc Natl Acad Sci U S A *104*, 3603-3608.

Quick, M., Yano, H., Goldberg, N.R., Duan, L., Beuming, T., Shi, L., Weinstein, H., and Javitch, J.A. (2006). State-dependent conformations of the translocation pathway in the tyrosine transporter Tyt1, a novel neurotransmitter:sodium symporter from *Fusobacterium nucleatum*. J Biol Chem *281*, 26444-26454.

Schaffner, W., and Weissmann, C. (1973). A rapid, sensitive, and specific method for the determination of protein in dilute solution. Anal Biochem *56*, 502-514.

Singh, S.K., Yamashita, A., and Gouaux, E. (2007). Antidepressant binding site in a bacterial homologue of neurotransmitter transporters. Nature *448*, 952-956.

Yamashita, A., Singh, S.K., Kawate, T., Jin, Y., and Gouaux, E. (2005). Crystal structure of a bacterial homologue of Na^+/Cl^--dependent neurotransmitter transporters. Nature *437*, 215-223.

Zhang, Y.W., and Rudnick, G. (2005). Cysteine-scanning mutagenesis of serotonin transporter intracellular loop 2 suggests an alpha-helical conformation. J Biol Chem *280*, 30807-30813.

Zomot, E., Bendahan, A., Quick, M., Zhao, Y., Javitch, J.A., and Kanner, B.I. (2007). Mechanism of chloride interaction with neurotransmitter:sodium symporters. Nature *449*, 726-730.